arXiv:1101.5155v2 [astro-ph.CO] 2 Jun 2011

A COSMIC COINCIDENCE: THE POWER-LAW GALAXY CORRELATION FUNCTION

Douglas F. Watson and Andreas A. Berlind[1],
Department of Physics and Astronomy, Vanderbilt University, Nashville, TN 37235

Andrew R. Zentner
Department of Physics and Astronomy, The University of Pittsburgh, Pittsburgh, PA 15260
Draft version June 3, 2011

ABSTRACT

We model the evolution of galaxy clustering through cosmic time to investigate the nature of the power-law shape of $\xi(r)$, the galaxy two-point correlation function. While $\xi(r)$ on large scales is set by primordial fluctuations, departures from a power law are governed by galaxy pair counts on small scales, subject to non-linear dynamics. We assume that galaxies reside within dark matter halos and subhalos. Therefore, the shape of the correlation function on small scales depends on the amount of halo substructure. We use a semi-analytic substructure evolution model to study subhalo populations within host halos. We find that tidal mass loss and, to a lesser extent, dynamical friction dramatically deplete the number of subhalos within larger host halos over time, resulting in a $\sim 90\%$ reduction by $z = 0$ compared to the number of distinct mergers that occur during the assembly of a host halo. We show that these non-linear processes resulting in this depletion are essential for achieving a power-law $\xi(r)$. We investigate how the shape of $\xi(r)$ depends on subhalo mass (or luminosity) and redshift. We find that $\xi(r)$ breaks from a power law at high masses, implying that only galaxies of luminosities $\lesssim L_*$ should exhibit power-law clustering. Moreover, we demonstrate that $\xi(r)$ evolves from being far from a power law at high redshift, toward a near power-law shape at $z = 0$. We argue that $\xi(r)$ will once again evolve away from a power law in the future. This is in large part caused by the evolving competition between the accretion and destruction rates of subhalos over time, which happen to strike just the right balance at $z \approx 0$. We then investigate the conditions required for $\xi(r)$ to be a power law in a general context. We use the halo model along with simple parametrizations of the halo occupation distribution (HOD) to probe galaxy occupation at various masses and redshifts. We show that key ingredients determining the shape of $\xi(r)$ are the fraction of galaxies that are satellites, the relative difference in mass between the halos of isolated galaxies and halos that contain a single satellite on average, and the rareness of halos that host galaxies. These pieces are intertwined and we find no simple, universal rule for which a power-law $\xi(r)$ will occur. However, we do show that the physics responsible for setting the galaxy content of halos do not care about the conditions needed to achieve a power law $\xi(r)$ and these conditions are met only in a narrow mass and redshift range. We conclude that the power-law nature of $\xi(r)$ for L_* and fainter galaxy samples at low redshift is a cosmic coincidence.

Subject headings: cosmology: theory — dark matter — galaxies: halos — galaxies: structure — large-scale structure of universe

1. INTRODUCTION

The two-point correlation function of galaxies was measured four decades ago and found to be consistent with a $\xi(r) \propto r^{-2}$ power law (Totsuji & Kihara 1969; Peebles 1973; Hauser & Peebles 1973; Peebles & Hauser 1974; Peebles 1974). Since that time, successively larger galaxy redshift surveys (e.g., Huchra et al. 1983; da Costa et al. 1988; Santiago et al. 1995; Shectman et al. 1996; Saunders et al. 2000; Colless et al. 2001; York et al. 2000) have mapped the distribution of galaxies with ever increasing precision and confirmed correlation functions consistent with power laws over a large range of scales (e.g., de Lapparent et al. 1988; Marzke et al. 1995; Hermit et al. 1996; Tucker et al. 1997; Jing et al. 1998, 2002; Norberg et al. 2002; Zehavi et al. 2002). The scales on which a single power-law description is valid span a range from large regions

exhibiting mild density fluctuations ($r \gtrsim 10$ Mpc), to smaller regions with large density fluctuations experiencing rapid non-linear evolution ($r \sim 1 - 10$ Mpc), to collapsed and virialized galaxy groups and clusters ($r \lesssim 1$ Mpc). It has long been noted that the lack of any feature delineating the transitions among these scales is surprising (e.g., Peebles 1974; Gott & Turner 1979; Hamilton & Tegmark 2002; Masjedi et al. 2006; Li & White 2009). This is especially true given that the matter correlation function in the now well-established concordance cosmological model differs significantly from a power law. In this paper, we return to this longstanding problem and address the origin of a power-law galaxy correlation function in the context of our modern paradigm for the growth of cosmic structure.

This conundrum can be refined within the contemporary framework in which galaxies live within virialized halos of dark matter (White & Rees 1978; Blumenthal et al. 1984). In such a model, galaxy clustering statistics can be modeled as a combination of dark

---

[1] Alfred P. Sloan Fellow

matter halo properties and a halo occupation distribution (HOD) that specifies how galaxies occupy their host halos (e.g., Peacock & Smith 2000; Scoccimarro et al. 2001; Berlind & Weinberg 2002; Cooray & Sheth 2002). In this *halo model* approach, the galaxy correlation function is a sum of two terms: On small scales, pairs of galaxies reside in the same host dark matter halo (the "one-halo" term), whereas on large scales, the individual galaxies of a pair reside in distinct halos (the "two-halo" term). These two terms depend on the HOD in different ways, requiring delicate tuning in order to spawn an unbroken power law (e.g., Berlind & Weinberg 2002). Consequently, a feature in $\xi(r)$ at scales corresponding to the radii of the typical, virialized halos that host luminous galaxies is expected.

In a dramatic success for the halo model, Zehavi et al. (2004) first detected a statistically-significant departure from a power law due to the high precision measurements of the Sloan Digital Sky Survey, and demonstrated that the halo model provides an acceptable fit to the data. Zehavi et al. (2005) confirmed this result, adding that power-law departures grow stronger with galaxy luminosity (see also Blake et al. 2008; Ross et al. 2010). $\xi(r)$ has since been shown to deviate from a power law at high redshifts (Ouchi et al. 2005; Lee et al. 2006; Coil et al. 2006; Wake et al. 2011). Nevertheless, it remains a fact that deviations from a power law at low redshifts are small and the galaxy correlation function is roughly a power law over an enormous range of galaxy-galaxy separations. Deviations have been revealed only through ambitious observational efforts.

Halos are known to be replete with self-bound structures, dubbed "subhalos" (Ghigna et al. 1998; Klypin et al. 1999; Moore et al. 1999), and both halos and subhalos are thought to be the natural sites of galaxy formation. Subhalos were isolated halos in their own right, hosting distinct galaxies before merging into a larger group or cluster halo[1]. Remarkably, the clustering of host halos along with their associated subhalos is very similar to that of observed galaxies (Kravtsov & Klypin 1999; Colín et al. 1999; Kravtsov et al. 2004a), suggesting a simple correspondence of galaxies with host halos and subhalos. This was clearly demonstrated by Conroy et al. (2006) who compared the correlation functions of hosts and subhalos to that of galaxies over a broad range of luminosities and redshifts ($z \sim 0 - 4$), finding excellent agreement. These results indicate that an understanding of the physics governing the subhalo populations within host halos may provide insight into the physics of galaxy clustering and the near power-law form of the galaxy two-point correlation function.

In this paper, we examine the causes of the observed power-law correlation function by studying the mergers, survival, and/or destruction of dark matter subhalos. Our focus in this paper is on the gross features of the galaxy two-point function and *not* on detailed comparisons to specific data sets. We explore more sophisticated galaxy-halo assignments and statistical comparisons with data in a forthcoming follow-up study (Watson et al. in prep.).

We argue that the nearly power-law, low-redshift galaxy correlation function is a coincidence. The correlation function of common $L \lesssim L_*$ galaxies evolves from relatively strong small-scale clustering at early times, through a power-law at the present epoch, and most likely toward relatively weak small-scale clustering in the future. The origin of the present-day power law, in turn, relies on the tuning of several disconnected ingredients, at least three of which are: the normalization of primordial density fluctuations determined by early Universe physics; a halo mass scale for efficient galaxy formation determined largely by atomic physics, stellar physics, and the physics of compact objects; and relative abundances of baryonic matter, dark matter, and dark energy in the Universe.

Our paper is organized as follows. In § 2.1 we review the halo model and restate the problem in terms of this framework. In § 3 we give an overview of our primary modeling technique. In § 4 we investigate the individual roles of merging, dynamical friction, and mass loss in shaping the halo occupation statistics of subhalos, as well as the resulting halo correlation function. In § 5 we show how $\xi(r)$ depends on host halo mass and redshift. In § 6 we explore a standard parametrization of the HOD to see what is required to get a power-law $\xi(r)$, and we predict the masses and redshifts at which a power-law $\xi(r)$ can be constructed. In § 7 we give a summary of our results and our primary conclusions. Throughout this paper, we work within the standard, vacuum-dominated, cold dark matter (ΛCDM) cosmological model with $\Omega_{\rm m} = 0.3$, $\Omega_{\Lambda} = 0.7$, $\Omega_{\rm b} = 0.04$, $h_0 = 0.7$, $\sigma_8 = 0.9$, and $n_{\rm s} = 1.0$. These values differ slightly form the WMAP best-fit values, however this has little effect on our general results and was chosen in order to compare to previous work that used similar cosmological models.

2. A MODERN RESTATEMENT OF THE PROBLEM IN HALO MODEL LANGUAGE

Though the observed galaxy correlation function is nearly a power law, the matter correlation function predicted by the concordance cosmological model is not. This is evident in Figure 1. On scales corresponding to collapsed objects, the dark matter correlation function exceeds the values that would be obtained by extrapolating the larger-scale power law to small scales. However, galaxies are biased with respect to dark matter in such a way as to counteract this excess. We can examine this discrepancy in terms of the halo model. If the reader is familiar with the halo model formalism, he or she may wish to skip to § 2.2

2.1. *Halo Model Basics*

Assuming that all galaxies live within virialized dark matter halos, the galaxies comprising any pair can come either from within the same halo (the *one-halo term*) or from two separate halos (the *two-halo term*). The correlation function is then given as the sum of these two terms

$$\xi(r) = \xi(r)^{\rm 1h} + \xi(r)^{\rm 2h} + 1, \qquad (1)$$

(e.g., Cooray & Sheth 2002; for this particular form of the equation see Zheng 2004). The probability distribution $P(N|M)$ that a halo of mass M contains N galaxies

---

[1] *Satellites* or *subhalos* are used throughout the paper to refer to self-bound entities lying within the virial radius of a larger halo. Those that do not lie within a larger system are designated as *centrals*, *host halos* or simply *hosts*.
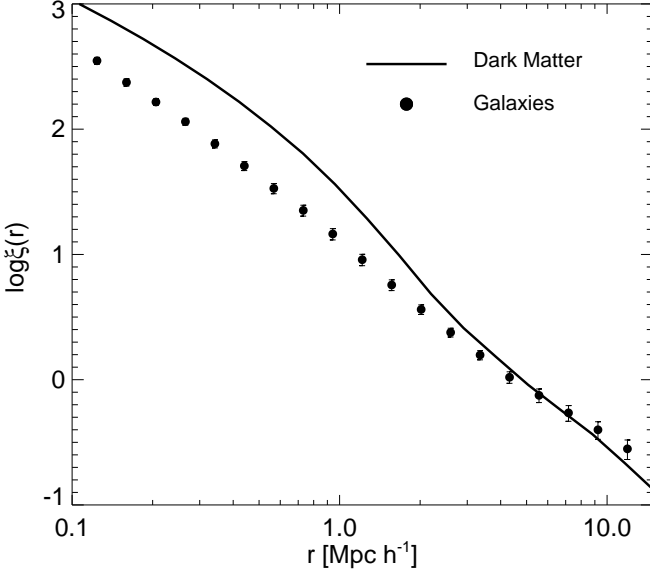
FIG. 1.— Correlation function of galaxies compared to dark matter. Points show the correlation function of galaxies from the APM survey, estimated from deprojecting the angular correlation function (Maddox et al. 1990; Baugh 1996). The curve shows the correlation function of dark matter measured from the LCDM GIF simulation run by the Virgo collaboration (Jenkins et al. 1998).

together with the spatial distribution of galaxies within their host halos constitute the *halo occupation distribution* (HOD). We denote the first and second moments of $P(N|M)$ at a specific mass M as $\langle N \rangle_M$ and $\langle N(N-1) \rangle_M$, respectively. The one-halo term can be computed by counting the average number of galaxy pairs of a given separation in a common halo and averaging over all halos. We write the one-halo term as (Berlind & Weinberg 2002)

$$1 + \xi(r)^{1h} = \frac{1}{2\pi r^2 \bar{n}_g^2} \int dM \frac{dn}{dM} \qquad (2)$$

$$\times \frac{\langle N(N-1) \rangle_M}{2} F(r|M)$$

where dn/dM is the halo mass function, $\langle N(N-1) \rangle_M/2$ is the mean number of galaxy pairs within a halo of mass M, and $F(r|M)$ is the distribution of separations between these pairs[2]. If the average spatial distribution of galaxies within their host halos is $\lambda(r|M)$, then the pair separation distribution $F(r|M)$ is the convolution of $\lambda(r|M)$ with itself. The quantity $\bar{n}_g$ is the mean density of galaxies in the Universe,

$$\bar{n}_g = \int dM \frac{dn}{dM} \langle N \rangle_M. \qquad (3)$$

Motivated by theoretical considerations (e.g., Berlind et al. 2003; Kravtsov et al. 2004a; Zheng et al. 2005), the HOD of galaxies is usually considered separately for central galaxies that live near the centers of their host halos and satellite galaxies that orbit within the host halo potential. Each halo above some mass

[2] This notation is slightly different from that used in Berlind & Weinberg (2002), in which $F(r)$ denoted the *cumulative* pair distribution.

threshold should contain one central galaxy and possibly one or more satellites, depending on the host mass and the HOD. In this framework it is useful to consider contributions to the one-halo term separately for central-satellite and satellite-satellite pairs. Therefore, we rewrite the one-halo term as (Berlind & Weinberg 2002)

$$1 + \xi(r)^{1h} = \frac{1}{2\pi r^2 \bar{n}_g^2} \int dM \frac{dn}{dM} \qquad (4)$$

$$\times \left[\langle N_{cen} N_{sat} \rangle_M F_{cs}(r|M) + \frac{\langle N_{sat}(N_{sat}-1) \rangle_M}{2} F_{ss}(r|M) \right],$$

where $\langle N_{cen} N_{sat} \rangle_M$ and $\langle N_{sat}(N_{sat}-1) \rangle_M/2$ are the mean number of central-satellite and satellite-satellite pairs in hosts of mass M, and $F_{cs}(r|M)$ and $F_{ss}(r|M)$ are the pair separation distributions of central-satellite and satellite-satellite pairs, respectively. If the central galaxies always reside very close to the center of the host halo and the average distribution of satellite positions within the host halo is $\lambda_s(r|M)$, then $F_{cs} = \lambda_s(r|M)$ and $F_{ss}(r|M)$ is the convolution of $\lambda_s(r|M)$ with itself. In practical cases there is at most one central galaxy and satellites are only present in halos with a central, so that $\langle N_{cen} N_{sat} \rangle_M = \langle N_{sat} \rangle_M$. The total fraction of galaxies that are satellites in a sample is then

$$f_{sat} = \bar{n}_g^{-1} \int dM \frac{dn}{dM} \langle N_{sat} \rangle_M$$

$$= \frac{\int dM \frac{dn}{dM} \langle N_{sat} \rangle_M}{\int dM \frac{dn}{dM} (\langle N_{cen} \rangle_M + \langle N_{sat} \rangle_M)}. \qquad (5)$$

The satellite fraction, f_{sat}, will prove an important quantity in determining the shape of the galaxy correlation function.

On scales significantly larger than individual halos, the two-halo term dominates the clustering strength. It is most simply written in Fourier space as (Cooray & Sheth 2002; for this particular form of the equation see Tinker et al. 2005)

$$P^{2h}(k) = P_m(k) \left[\bar{n}_g^{-1} \int dM \frac{dn}{dM} \langle N \rangle_M \right. \qquad (6)$$

$$\left. \times b_h(M,r) \tilde{\lambda}(k|M) \right]^2,$$

where $P_m(k)$ is the matter power spectrum, $b_h(M,r)$ is a (possibly scale-dependent) halo bias function, and $\tilde{\lambda}(k|M)$ is the Fourier transform of the spatial number density of galaxies within their host halos. We can invert the Fourier transform of the two-halo power spectrum to recover the two-halo term of the correlation function. In the limit that the galaxy pair separation is larger than any halo of interest, the two-halo term becomes

$$\xi^{2h}(r) \simeq \left[\bar{n}_g^{-1} \int b_h(M,r) \langle N \rangle_M \frac{dn}{dM} \, dM \right]^2 \xi_m, \qquad (7)$$

$$= b_g^2 \, \xi_m,$$

where $\xi_m(r)$ is the matter correlation function. Equation (7) explicitly shows that the large-scale galaxy correlation function is essentially the halo correlation function except halos of different masses are weighted by

$\langle N \rangle_M$. The galaxy bias describing the relative clustering of galaxies to dark matter $b_{\mathrm{g}} = \sqrt{\xi/\xi_m}$ is the quantity in square brackets in Equation (7).

2.2. *The Battle of the 1- Halo and 2- Halo Terms*

Berlind & Weinberg (2002) showed that maintaining a power-law correlation function requires a careful balance between the one-halo and two-halo terms and is thus quite difficult to achieve. This is because the one-halo term generally changes by a larger amount than the two-halo term in response to changes to the HOD. A close examination of Equations (3), (4), (6) and (7) reveals why this is the case.

Consider first the two-halo term as it is the simplest. On large scales, the two-halo term is just a weighted average of the clustering of host halos. For simplicity, assume (albeit incorrectly) the halo bias to be a constant function of halo mass. Increasing $\langle N \rangle_M$ increases both the number of two-halo pairs at a given separation (the square of the integral in Eqs. [6] and [7]) and the number of random pairs $\bar{n}_{\mathrm{g}}^2/2$, by the same amount. The reason the two-halo term is at all sensitive to the HOD is that the bias of halos does depend on mass and so changing the relative number of galaxies in high-mass vs. low-mass halos changes the weight in the average of the halo bias in Equation (7). For example, assigning a large number of satellite galaxies to high-mass halos increases $\xi^{2\mathrm{h}}(r)$ by weighting highly-biased, high-mass halos more heavily. The possible range in the amplitude of the two-halo term is limited by the variation of the halo bias function $b_h(M)$, within the mass range relevant to galaxies, $10^{11} \lesssim M/M_\odot \lesssim 10^{15}$. At low masses, the halo bias is $b_h \sim 0.65$ while, in the cluster regime ($M \sim 10^{14}h^{-1}M_\odot$), it grows to values of $b_h \sim 2$ (Tinker et al. 2005). Bias continues to grow with mass, but more massive halos are rare and do not contribute much to the weighted average because dn/dM is miniscule. The two-halo term scales like the square of the average bias b_{g} in Equation (7), so the possible dynamic range $\xi^{2\mathrm{h}}$ can display is, at most, a factor of ~ 9 and is usually significantly smaller. Simply put, the two-halo term depends weakly on the HOD because on large scales it is not possible to make galaxies significantly more or less clustered than the host halos they occupy.

On small scales, the one-halo term dominates and the situation is different. The number of galaxy pairs within an individual halo scales with $\langle N(N-1) \rangle_M$ while the number of random pairs scales with $\bar{n}_{\mathrm{g}}^2$, or $\langle N \rangle_M^2$. It is instructive to break the HOD into central and satellite galaxies. In the regime where there is one central galaxy per halo, the mean number of central-satellite pairs is $\langle N_{\mathrm{cen}}N_{\mathrm{sat}} \rangle_M = \langle N_{\mathrm{sat}} \rangle_M$, whereas the mean number of satellite-satellite pairs is $\langle N_{\mathrm{sat}}(N_{\mathrm{sat}}-1) \rangle_M/2$. Assuming a Poisson distribution for the number of satellite galaxies (Kravtsov et al. 2004a), $\langle N_{\mathrm{sat}}(N_{\mathrm{sat}}-1) \rangle_M = \langle N_{\mathrm{sat}} \rangle_M^2$. The mean number of random pairs scales like $(1 + \langle N_{\mathrm{sat}} \rangle)_M^2$. In the limit $\langle N_{\mathrm{sat}} \rangle_M \gg 1$, the number of satellite-satellite pairs dominates the number of central-satellite pairs, but in this limit both the number of one-halo pairs and the square of the mean galaxy number density scale as $\langle N_{\mathrm{sat}} \rangle_M^2$ so the one-halo term saturates to a maximum value and is insensitive to the number of satellite galaxies per halo.

In most practical cases, the fraction of satellite galaxies in an observational sample is $f_{\mathrm{sat}} \lesssim 0.25$, so samples tend to be dominated by halos with satellite galaxy populations in the opposite limit, $\langle N_{\mathrm{sat}} \rangle_M \ll 1$. This is due to the fact that very massive host halos are rare, so halos with $\langle N_{\mathrm{sat}} \rangle_M > 1$ are rare. With $\langle N_{\mathrm{sat}} \rangle_M \ll 1$, the central-satellite term dominates and the number of such pairs scales as $\langle N_{\mathrm{sat}} \rangle_M$ while the mean number density $\bar{n}_{\mathrm{g}}$ is approximately constant. Examination of Equations (4) and (5) reveals that in this regime $\xi^{1\mathrm{h}}$ scales *in proportion to the fraction of satellite galaxies and in inverse proportion to the number of host halos*. Host halo mass is largely fixed by requiring the galaxies in any sample to have an appropriate average number density (this is why rare galaxies exhibit strong small-scale clustering). Therefore, the one-halo term describing any given sample varies approximately linearly with $\langle N_{\mathrm{sat}} \rangle_M$ until $\langle N_{\mathrm{sat}} \rangle > 1$, at which point it saturates. It is interesting that nearly all the sensitivity of the correlation function to the HOD comes from central-satellite galaxy pairs in host halos where satellite galaxies are uncommon!

In this work, we aim to understand the origin of the nearly power-law galaxy correlation function. The relevant question is why is it that the number of galaxies (or satellite galaxies to be more specific) per halo is set just so that the one-halo and two-halo terms in the galaxy correlation function match smoothly, leaving only small deviations from a single power law over several orders of magnitude in scale? We confront this problem by studying the properties and evolution of subhalo populations. We now turn to some of the details of our modeling methods.

3. OVERVIEW OF HALO SUBSTRUCTURE MODELING

Our approach is to study the evolution of subhalos within virialized host halos as a method to understand satellite galaxies and, in turn, the evolution of galaxy clustering. We focus our attention on the relative strengths of small-scale and large-scale clustering. We study subhalo populations using the approximate semi-analytic model of Zentner et al. (2005, hereafter Z05). In this section, we briefly review the fundamental aspects of the model that are of immediate relevance and we refer the reader to Z05 for details and validation. The subhalo model is based on Zentner & Bullock (2003) and is similar to the independent models of Taylor & Babul (2004, 2005a,b) and Peñarrubia & Benson (2005), while sharing many features with other approximate treatments of halo substructure (Oguri & Lee 2004; van den Bosch et al. 2005; Faltenbacher & Mathews 2005; Purcell et al. 2007; Giocoli et al. 2008, 2009).

Semi-analytic models are an approximation to the calculations of large N-body simulations, yet such models offer many advantages: (1) semi-analytic calculations are computationally inexpensive; (2) they have no inherent resolution limits; (3) they enable the statistical study of subhalos within very large numbers of host halos; (4) they allow the growth and mass-loss histories of particular subhalos to be tracked without significant post-processing and analysis; (5) they make studies of model parameter space tractable; and (6) semi-analytic models facilitate parsing complex physical phenomena so that the relative importance of different physical effects may be understood. Our goal is to quantify the

relative importance of merging, which increases subhalo abundances, and dynamical friction and mass loss, which decrease subhalo abundances. We also aim to explore predictions for subhalo populations and galaxy correlation functions from high redshift to several Hubble times in the future. Z05 extensively tested the model we use in this paper and showed that the model produces subhalo mass functions, occupation statistics, and radial distributions within hosts that are in good agreement with a number of high-resolution N-body simulations (see the recent comparison in Koushiappas et al. 2010, as well).

The analytic model proceeds in several steps. For a host halo of a given mass M, observed at a given redshift z, we generate a halo merger tree using the mass-conserving implementation of the excursion set formalism (Bond et al. 1991; Lacey & Cole 1993, 1994) developed by Somerville & Kolatt (1999, see Zentner 2007 for a review). This yields a complete history of the masses and redshifts of all halos that merged to form the final, target halo of mass M at redshift z. The host halo is the largest halo at each point in the merger tree. We model the density distributions of all halos as Navarro et al. (1997, hereafter NFW) profiles with concentrations determined by their merger histories according to Wechsler et al. (2002). At the time of each merger, we assign the subhalo initial orbital parameters drawn from distributions measured in N-body simulations (Z05, see Benson 2005 for similar formalisms). We then integrate each subhalo orbit within the host halo gravitational field, taking into account dynamical friction and mass loss. We estimate dynamical friction with an updated form of the Chandrasekhar (1943) approximation (Hashimoto et al. 2003; Zentner & Bullock 2003), account for internal heating so that scaling relations describing the internal structures of subhalos are obeyed (Hayashi et al. 2003; Kazantzidis et al. 2004; Kravtsov et al. 2004b), and allow for loss of material beyond the tidal radius on a timescale comparable to the local dynamical time. The details of each ingredient are given in Z05.

The correlation function of halos and subhalos and their associated galaxies is sensitive to the abundance of subhalos that survive both possible mergers with the central, host galaxy due to dynamical friction as well as mass loss and thus remain as distinct objects in orbit within their host halos with their galaxies intact. Therefore, it is necessary to specify conditions under which the galaxy within a subhalo may be "destroyed" and removed from our samples. In this work, we consider the clustering of mass-threshold samples of halos and subhalos as a proxy for luminosity-threshold samples of galaxies, so significant mass loss will lead to a galaxy that is either destroyed or dropped out of our sample. We assume such a scaling between halo mass and galaxy luminosity *solely for the sake of simplicity.* Our primary points are qualitative in nature, but we note that this is similar to other schemes that have described data successfully (e.g., Kravtsov & Klypin 1999; Colín et al. 1999; Kravtsov et al. 2004a; Tasitsiomi et al. 2004; Conroy et al. 2006) and our calculations with similar, but more sophisticated assignments do not alter any of our basic results or conclusions. In rare cases, subhalos may survive close encounters with the center of their host halo potentials. We remove all subhalos that have orbital

apocenters $r_{\rm apo} < 5$ kpc. This choice is physically motivated because the galaxies within such subhalos would likely have merged with the central galaxy, or at least be observationally indistinguishable from the central galaxy. This choice is relatively conservative in that galaxies on larger orbits would also likely be influenced and it only affects the results of calculations in which tidal mass loss is not permitted (see below). The net result of evolving orbits for each subhalo in the merger tree is a catalog of all surviving subhalos in the final host halo at the time of observation. In some cases, a halo that merges into a larger host contains subhalos of its own. These subs-of-subs are only abundant inside very large host masses and are present in our model.

One of our aims is to study the individual roles of halo merging, dynamical friction, and mass loss on the clustering of halos. Therefore, we compute subhalo populations in four different sets of circumstances:

No Effects - a "bare-bones" model that does not allow satellite galaxies to be modified by dynamical friction or mass loss. In this case, any infalling subhalo remains intact, and we assume that this subhalo harbors a galaxy that will survive forever. This is tantamount to assuming that galaxies form in all sufficiently-large peaks in the primordial density field and survive until today.

Fric. Only - a model that only considers the effects of halo merging and dynamical friction. Subhalos never lose mass and can only be destroyed by sinking to the very centers of their hosts.

Strip. Only - a model that only considers halo merging and mass loss and assumes no dynamical friction or central merging. Subhalos can lose mass and drop out of a mass threshold sample, but they cannot lose orbital energy and sink to the center of the host potential.

Full - our full model treating halo merging, dynamical friction, and mass loss. This is the model that was developed in Z05 and validated against N-body simulations.

We run our models for host masses[3] in the range from $\log(M_{\rm host}/h^{-1}M_\odot) = 11.0$ to 15.0 in steps of $\Delta(\log M_{\rm host}) = 0.1$. For each of these masses, we run 1000 statistical model realizations representing different realizations of the local density field and different halo merger histories. In this way, we sample the statistical properties of subhalo populations over the entire range of host halo masses relevant to galaxy-galaxy correlations. We repeat this process for host masses at $z = 0$ as well as two past redshifts, $z = 3$ and $z = 1$, and two future redshifts, $z = -0.6$, and $z = -0.9$.

4. EFFECTS OF SUBHALO DYNAMICS ON THE GALAXY CORRELATION FUNCTION

4.1. *Halo Occupation Distribution Statistics*

[3] We note that we use the "virial" definition of a halo in which a halo is defined as a spherical region of mean density equal to $\Delta_{\rm vir}$ times the mean background density. For our cosmological model, $\Delta_{\rm vir} = 337$ at $z = 0$ and approaches 178 at high z.

The galaxy correlation function may be considered primarily a function of the galaxy HOD (e.g., Berlind & Weinberg 2002). The prevailing cosmological model is now stringently constrained and may be considered fixed for our purposes. Moreover, theoretical predictions of the abundances, clustering, and structures of host dark matter halos in the concordance cosmology are now well established. Consequently, we focus on the properties of the HOD and the manner in which the HOD determines galaxy clustering.

We expect that each host halo of sufficient size contains one dominant, central galaxy associated with the host itself, as well as additional satellite galaxies that are associated with relatively large subhalos. Thus, the HOD of galaxies should resemble the HOD of all halos (hosts plus their subhalos), and such a model is bolstered by significant empirical support (Kravtsov & Klypin 1999; Colín et al. 1999; Kravtsov et al. 2004a; Tasitsiomi et al. 2004; Conroy et al. 2006). As a result, we concentrate on the insight that can be gleaned about the development of the HOD of all halos, paying particular attention to the separate effects of halo mergers, dynamical friction, and mass loss.

The left column of Figure 2 shows the mean occupation number of host halos and subhalos as a function of host halo mass $\langle N \rangle_M$, at $z = 0$. The three panels give results for halo samples defined by different mass thresholds. In the interest of simplicity, we assume that all host halos and surviving subhalos with masses $M \geq M_{\min}$ harbor an observable galaxy. This assignment is simpler than those supported by detailed comparisons to data, which typically assume that all host halos and surviving subhalos with masses $M \geq M_{\min}$ (or some maximum circular velocity) *at the epoch of accretion* harbor an observable galaxy. We proceed in this manner because the subtleties discussed in the aforementioned literature do not influence our primary points and may serve to obscure them. This is primarily because any mass threshold chosen at the epoch of accretion will have a second "destruction" threshold due to the finite resolution of a given N-body simulation. This can alter clustering measurements, and since the aim of this paper is to present the qualitative trends responsible for the low-redshift correlation function, we use the simpler final mass approximation. We have confirmed that using mass at accretion with our model reproduces the same general results. In a forthcoming paper we consider more sophisticated models to compare with data. In the top, middle, and bottom panels we show samples with $\log(M_{\min}/h^{-1}M_{\odot}) = 11.4$, 11.7, and 12.3, respectively. These particular mass thresholds result in average galaxy number densities (see Eq. [3]) equal to those in observed SDSS samples with r-band luminosity thresholds of $M_r < -18.5$, -19.5, and -20.5 (Zehavi et al. 2005). The four curves in each panel represent the four model modes described in § 3, and we calculate each curve from the mean of the 1000 model realizations.

First, the black dot-dashed curves represent the *No Effects* model. As explained in § 3, this model assumes that any halo that merges into a larger host system (and becomes a subhalo of that system) is thereafter unaltered by dynamical effects in the host halo environment. Physically, this corresponds to the simple (and observationally untenable) assumption that each subhalo above

$M_{\min}$ brings with it an observable galaxy upon merging into the host and that this galaxy is not destroyed or dimmed by dynamical evolution within the host halo. In effect, each local peak of sufficient mass in the smoothed density distribution forms a galaxy and the galaxy can not be destroyed. Of course, we expect the mean halo occupation in this model to be high for all host masses as compared to the other models.

Next, we turn to the curves depicting the individual effects of dynamical friction (*Fric. Only*, green dashed curves) and mass loss (*Strip. Only*, blue dotted curves). These dynamical mechanisms can destroy subhalos, but they cannot affect the host halo or central galaxy. This is why all the curves converge to the value $\langle N \rangle_M = 1$ at low host masses. As a convenient shorthand, we refer to any subhalo that fell into its host system with a mass $M_{\text{sub}} \geq M_{\min}$, but then merged with the central host galaxy or lost sufficient mass to fall below this threshold, as *destroyed*. This does not mean that the subhalo has become unbound, but merely that it has either merged or no longer has a bound mass above some minimum mass threshold.

Dynamical friction acting alone destroys subhalos by causing them to sink to the centers of their hosts and "merge" with it. This mechanism alone causes a 20-35% decrease in the mean number of surviving satellites for all host masses as compared to the *No Effects* model. The fractional decrease in subhalos depends only weakly on host mass, but a comparison of the different mass threshold panels shows a modest dependence on subhalo mass, with smaller mass subhalos being depleted more. These trends are counter-intuitive because the dynamical friction force is an increasing function of $M_{\text{sub}}/M_{\text{host}}$, the mass ratio between the subhalo and its host (Binney & Tremaine 2008). One might expect the depletion of subhalos to be larger for smaller host masses at fixed subhalo mass or for larger subhalo masses at fixed host mass. Our results differ from this expected behavior for two reasons. First and foremost, low-mass-ratio mergers tend to occur at higher redshifts than high-mass-ratio mergers. At higher redshifts, host halos are significantly smaller than they are at present, so high-redshift mergers probe only the dense interiors of contemporary host halos and evolve approximately according to the subhalo-host mass ratio at the redshift of the merger. These early-merging subhalos also have a longer period of time during which to evolve. Second, our models include subhalos-of-subhalos. As we move to larger host masses at fixed subhalo mass or smaller subhalo masses at fixed host mass, more subhalos are subs-of-subs that have much higher mass ratios with their immediate hosts. These effects result in the trends we see in Figure 2.

Mass loss is significantly more effective at "erasing" subhalos than dynamical friction. Mass loss processes can effectively "destroy" subhalos because many lose sufficient mass to fall below the threshold of a sample. This mechanism typically drives an 80-85% decrease in the number of objects above a given mass threshold compared to the *No Effects* model. Again, the fractional decrease in subhalos is nearly independent of host mass, but it shows a slight dependence on subhalo mass, with smaller mass subhalos being destroyed more efficiently.

Finally, the *Full* model (red, solid curves) includes the effects of both subhalo mass loss and orbital decay by
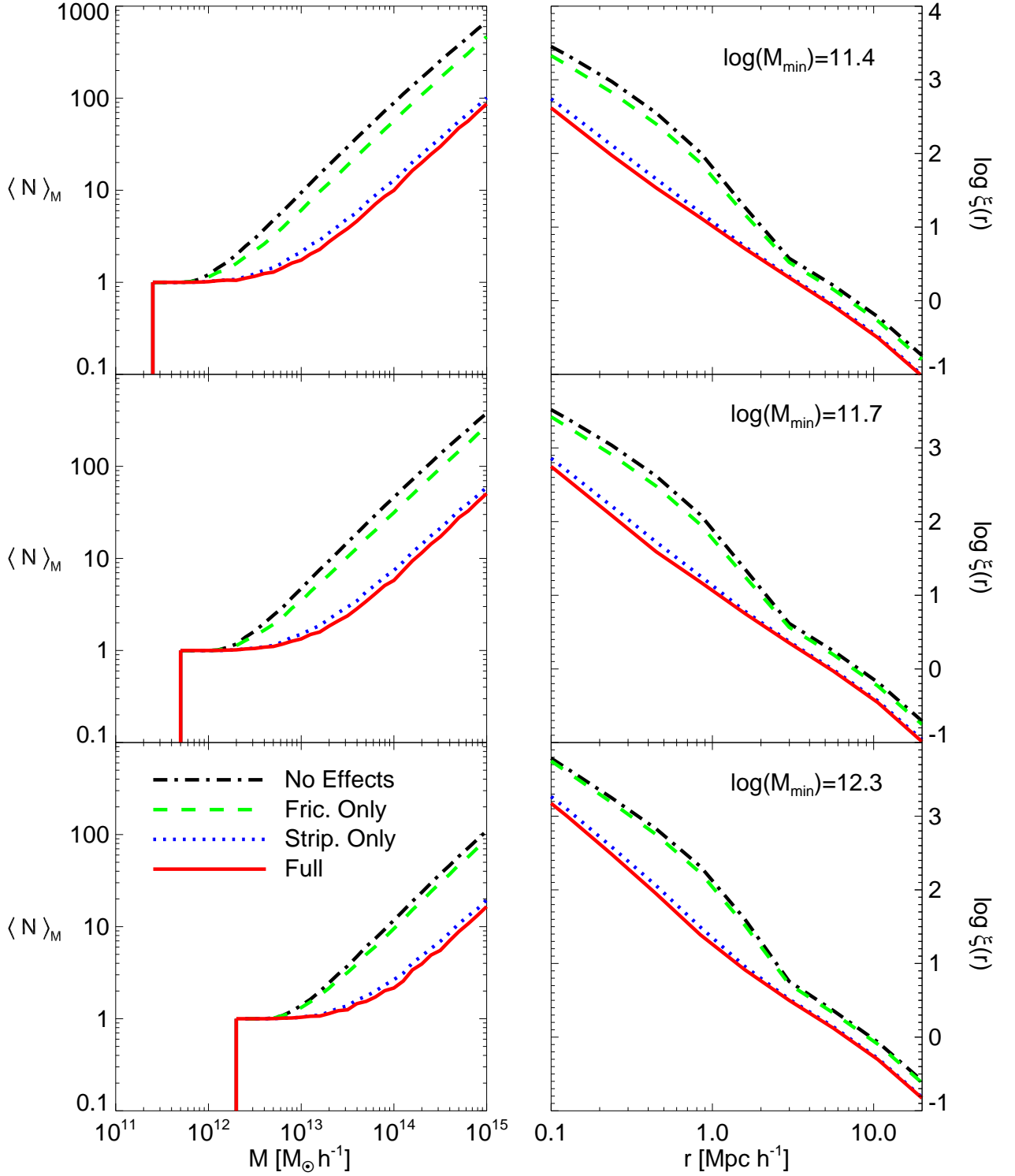
Fig. 2.— *Left Panels*: Mean number of all halos (hosts plus subhalos) predicted by our subhalo model as a function of host halo mass, at redshift $z = 0$. The three panels show results for three mass threshold values: $\log(M_{\min}/h^{-1}M_{\odot}) = 11.4, 11.7$, and 12.3. The four curves in each panel correspond to the four models described in § 3: *No Effects* considers no gravitational effects on subhalos as they orbit inside their host halos (black dot-dashed curve); *Fric. Only* considers only the effects of dynamical friction (green dashed curve); *Strip. Only* considers only the effects of mass loss (blue dotted curve); *Full* considers both dynamical friction and mass loss (solid red curve). *Right Panels*: The correlation function of all halos predicted by our subhalo model. $\xi(r)$ is computed from the halo model using the occupation statistics shown in the left panels. The figure shows that dynamical effects (especially mass loss) are needed in order to reduce the number of subhalos sufficiently and produce a power-law correlation function.

dynamical friction. These processes do not simply sum together. As a subhalo sinks deeper into its host potential well due to dynamical friction, it experiences a stronger tidal field and is thus more efficiently stripped of its mass. Conversely, less massive subhalos are less susceptible to orbital decay via dynamical friction. A comparison of the *Full* model to the *Strip. Only* model shows that including dynamical friction causes an additional $\sim 15\%$ depletion of substructure. Mass loss is by far the dominant cause of subhalo destruction. Overall, Figure 2 shows that dynamical effects reduce the number of subhalos by $\sim 90\%$ compared to the number of distinct mergers that occur during the formation of a host halo.

4.2. *Constructing the Correlation Function*

We use the halo model outlined in § 2.1 to compute the correlation function predicted by our subhalo model. Specifically, we use the Jenkins et al. (2001) mass function and we follow Tinker et al. (2005) in using the Smith et al. (2003) formula for the non-linear matter power spectrum and the Tinker et al. (2005) scale-dependent halo bias relative to the non-linear power spectrum. We derive HOD statistics from our subhalo models as exemplified by the previous section, and we compute the pair separation distributions by assuming that the radial distributions of satellites follows an NFW profile for simplicity. In actuality, the subhalo distributions in both our models and N-body simulations are slightly shallower than NFW (see Z05 for model and simulation results). We adopt the NFW profile for analytical convenience as deviations from NFW are small and only influence correlation functions notably on scales significantly smaller than $r \sim 100h^{-1}$kpc (e.g., Z05; also see Watson et al. 2010 for a demonstration of this point regarding satellite galaxies).

The right column of Figure 2 shows the host+subhalo correlation functions computed in this manner from the HODs predicted by our subhalo model. In the *No Effects* case, where no subhalos are destroyed, $\xi(r)$ is very different from a power law, having a one-halo term that is too large relative to the two-halo term so that a distinct feature is present in $\xi(r)$ on scales $r \sim 2$ Mpc. In fact, comparing this to Figure 1, we see that it is very similar to the dark matter correlation function. This is perhaps not surprising because subhalos in this model behave as massive test particles that cannot be altered. As dynamical effects are included and substructure is consequently depleted, $\xi(r)$ drops on all scales. Recall that only subhalos (hosting satellite galaxies) can be destroyed and the number of host galaxies remains unaltered. The fraction of all objects that are satellites therefore decreases. As we discussed in § 2.1, for a fixed population of central galaxies, the one-halo term drops in approximate proportion to the number of satellite galaxies. So as the number of satellites declines, so does the number of pairs within halos relative to the total number of pairs and the one-halo term declines.

Large-scale clustering is less sensitive to changes in the satellite galaxy population. The two-halo term drops because subhalos tend to populate more massive hosts (as in the left column of Figure 2), so the average host halo mass of a sample decreases as subhalos are depleted. The large-scale clustering strength of halos increases with

halo mass, so this depletion results in weaker large-scale clustering. The variability of the two-halo term is relatively mild because the halo bias is not a rapidly-varying function of halo mass near $M \sim M_{\min}$ (Tinker et al. 2005).

With enough depletion of substructure, the one- and two-halo terms align and result in a nearly power-law shape. This is exactly what happens in Figure 2. In our *Full* subhalo model the correlation function is roughly a power law. To obtain a nearly power-law galaxy correlation function, it is necessary that a majority of early galaxies and proto-galaxies that merge to form a massive system at low redshift be destroyed through either central mergers or mass loss. Our results suggest that mass loss is mainly responsible for this depletion, while dynamical friction and central galaxy mergers play a comparably small, supporting role. Incidentally, this picture implies that infalling satellite galaxies lose significant stellar mass so that they provide an important source of the diffuse intracluster light observed in galaxy groups and clusters and this picture is consistent with observations (Purcell et al. 2007, 2008). Comparing our correlation function results for the three different mass thresholds, we note that $\xi(r)$ is closer to a power law for lower-mass samples. We revisit this point in the next section.

We now return to the mean occupation statistics shown in the left panels of Figure 2. The so-called "plateau" region of the HOD is the flat region at $\langle N \rangle_M = 1$, where host halos are more massive than $M_{\min}$, but not yet massive enough to host subhalos above our mass threshold [4]. As substructure is depleted, the prominence of this plateau increases. The "length" of the plateau in the HOD can be expressed as the ratio between the mass of a halo that hosts a single satellite on average, M_1, to the minimum mass required to host a central galaxy, $M_{\min}$. Zehavi et al. (2005) fit an HOD model to the measured correlation function of SDSS galaxies and found that a ratio $M_1/M_{\min} \sim 23$ is consistent with clustering data, nearly independent of galaxy luminosity. In other words, a consistent picture is one in which the entire HOD shifts to higher masses in a self-similar manner, with $M_1/M_{\min}$ fixed, in order to accommodate higher-luminosity samples. Remarkably, Kravtsov et al. (2004a) studied this for subhalos in a high-resolution N-body simulation and found that $M_1/M_{\min} \sim 20$, regardless of $M_{\min}$ as well. Meanwhile, Tinker et al. (2005) fit a slightly more complex HOD model to the SDSS data and found that $M_1/M_{\min} \sim 25$ for galaxy samples with luminosities less than L_*, but decreases to $M_1/M_{\min} \lesssim 5$ to accommodate the highest-luminosity samples (absolute r-band magnitudes $M_r \leq -21$). The new analysis by Zehavi et al. (2010) also finds this trend with $M_1/M_{\min} \sim 17$ for $M_r \geq -20.5$ and much lower values for higher luminosity galaxies. For the purpose of comparison, the *Full* subhalo model shown in Figure 2 predicts $M_1/M_{\min} \sim 40$ for the low-mass samples of $\log(M_{\min}/h^{-1}M_\odot) = 11.4$ and $\log(M_{\min}/h^{-1}M_\odot) = 11.7$, and $M_1/M_{\min} \sim 30$ for the higher-mass sample of $\log(M_{\min}/h^{-1}M_\odot) = 12.3$.

These results suggest that getting the length of the

---

[4] Roughly speaking, the most massive subhalo within any host is a few percent of the mass of the host halo (e.g., Z05). This is the case with, for example, the Large Magellanic Cloud within the halo of the Milky Way (Busha et al. 2010).

HOD plateau right may be a key ingredient needed to establish a power-law correlation function and this has been part of the interpretation in the literature. The importance of $M_1/M_{\rm min}$ stems from the fact that most one-halo pairs reside in halos with average satellite numbers $\langle N_{\rm s} \rangle_M \lesssim 1$, so modeling the HOD at relatively low satellite occupation numbers is critical (see Conroy et al. 2006). We investigate this further in § 6.

5. MASS AND REDSHIFT DEPENDENCE OF THE CORRELATION FUNCTION

5.1. *Dependence on Mass*

While dynamical processes act in a manner to deplete substructure and push $\xi(r)$ toward a power law at all mass thresholds, it is evident that deviations from a power law are stronger with increasing host mass. Figure 3 shows the correlation functions predicted by our *Full* subhalo model for four different mass thresholds, ranging from $\log(M_{\rm min}/h^{-1}M_\odot) = 13.5$, corresponding to bright galaxies such as Luminous Red Galaxies (LRGs), down to $\log(M_{\rm min}/h^{-1}M_\odot) = 10.5$, corresponding to dwarf galaxies. While the correlation function of the "dwarf" sample is a near power law, that of the "LRG" sample exhibits strong departures from power-law behavior. This trend has been detected with SDSS galaxies by Zehavi et al. (2005) who found evidence that a power-law model provides a better fit to low-luminosity galaxies than high-luminosity galaxies. Halo and subhalo clustering exhibits the same trend. More massive halos contain slightly more of their bound masses in substructure relative to less massive halos, but this is a comparably small effect (Z05) and drives only $\sim 30\%$ of the mass-dependence of the one-halo term in Figure 3. At *fixed redshift*, the departure from a power-law at high mass (high luminosity) is caused by the relative rareness of high-mass host halos (see § 2.1 for interpretive discussion).

5.2. *Dependence on Redshift*

Substructure abundances vary with time. Infall of new subhalos acts as a "source" of halo substructure. The rate of mergers of halos into larger systems is a function of redshift that typically peaks at redshifts $z \sim 1 - 3$ in the halo mass range of interest and declines thereafter (Z05; Zentner 2007). Once a subhalo merges into a larger host halo, dynamical friction shrinks its orbit and the subhalo loses mass. Given enough time, the subhalo will eventually lose enough mass to fall below $M_{\rm min}$ or merge with the central galaxy and lose its identity. The balance between the halo merger rate and the rates of destructive processes (which occur on a halo dynamical time) determine the redshift dependence of halo substructure.

Figure 4 shows the redshift evolution of the mean halo occupation number and resulting correlation functions. The layout of Figure 4 is similar to that of Figure 2, with $\langle N \rangle_M$ shown in the left panels, $\xi(r)$ shown in the right panels. However, in Figure 4 all results are for the *Full* subhalo model, and the various lines denote quantities evaluated at different redshifts, $z = 3, 1, 0, -0.6, -0.9$ (where negative redshifts correspond to *future* epochs). Moreover, in each panel the correlation functions are scaled by a power law to better highlight departures from a power-law shape.
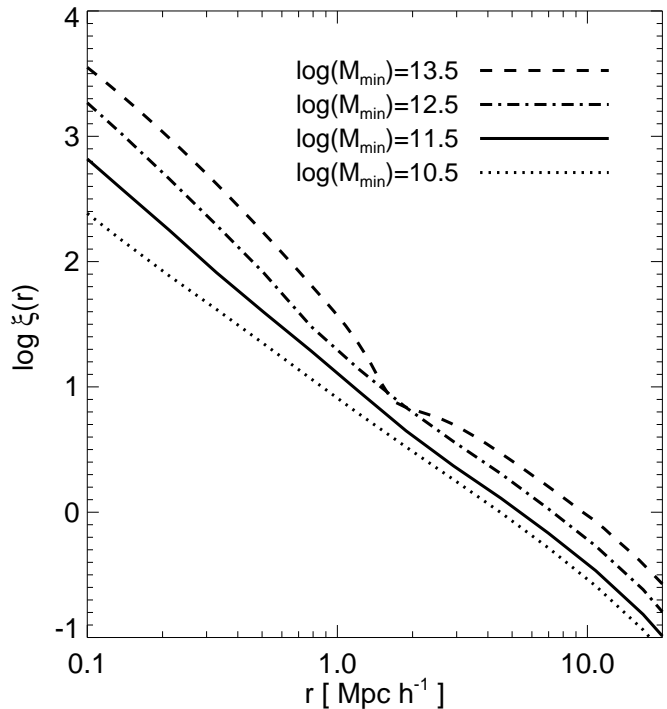

FIG. 3.— Correlation function of all halos (hosts plus subhalos) predicted by our subhalo model at redshift $z = 0$. The four curves show $\xi(r)$ for four mass threshold samples and the threshold values $M_{\rm min}$ (in units of $h^{-1}M_\odot$) are listed in the panel. The figure shows that $\xi(r)$ breaks more and more from a power law for higher mass halo samples, which correspond to higher luminosity galaxy samples.

The left-hand panels of Figure 4 show that the average number of subhalos within hosts of a given mass starts out high at early times and begins to decrease after $z = 3$, as merger rates decline. By the present epoch ($z = 0$), the number of subhalos has dropped by $\sim 25 - 30\%$ relative to what it was at $z = 3$. One Hubble time into the future ($z = -0.6$), the abundance of substructure has dropped by $\sim 60\%$. This is because the rate of merging as a source for new subhalos declines rapidly. This decrease in the merger rate is dictated in large part by the quenching of structure growth by the cosmological constant (Carroll et al. 1992), but also because most halos of interest are below the typical collapsing mass, which approaches $M_* \simeq 10^{14}\, h^{-1} {\rm M}_\odot$ in the future (Zentner 2007). Meanwhile, destructive processes continue to operate on orbiting halo substructure for several additional dynamical times. Three Hubble times into the future ($z = -0.9$) the average halo occupation has dropped by $\sim 90\%$. As with our previous results, the fractional decrease in subhalo abundance appears to be roughly independent of host mass, meaning that the slope of the HOD in the high-$\langle N \rangle_M$ limit is not significantly altered by evolution. The amplitude of $\langle N \rangle_M$ declines considerably, resulting in increasing $M_1/M_{\rm min}$, or a "lengthening" of the HOD plateau with time. This behavior is strikingly similar to that seen in Figure 2 in the sense that turning on dynamical effects at a fixed redshift has a qualitatively similar impact as evolving forward in time, and the effects on the correlation function are similar.
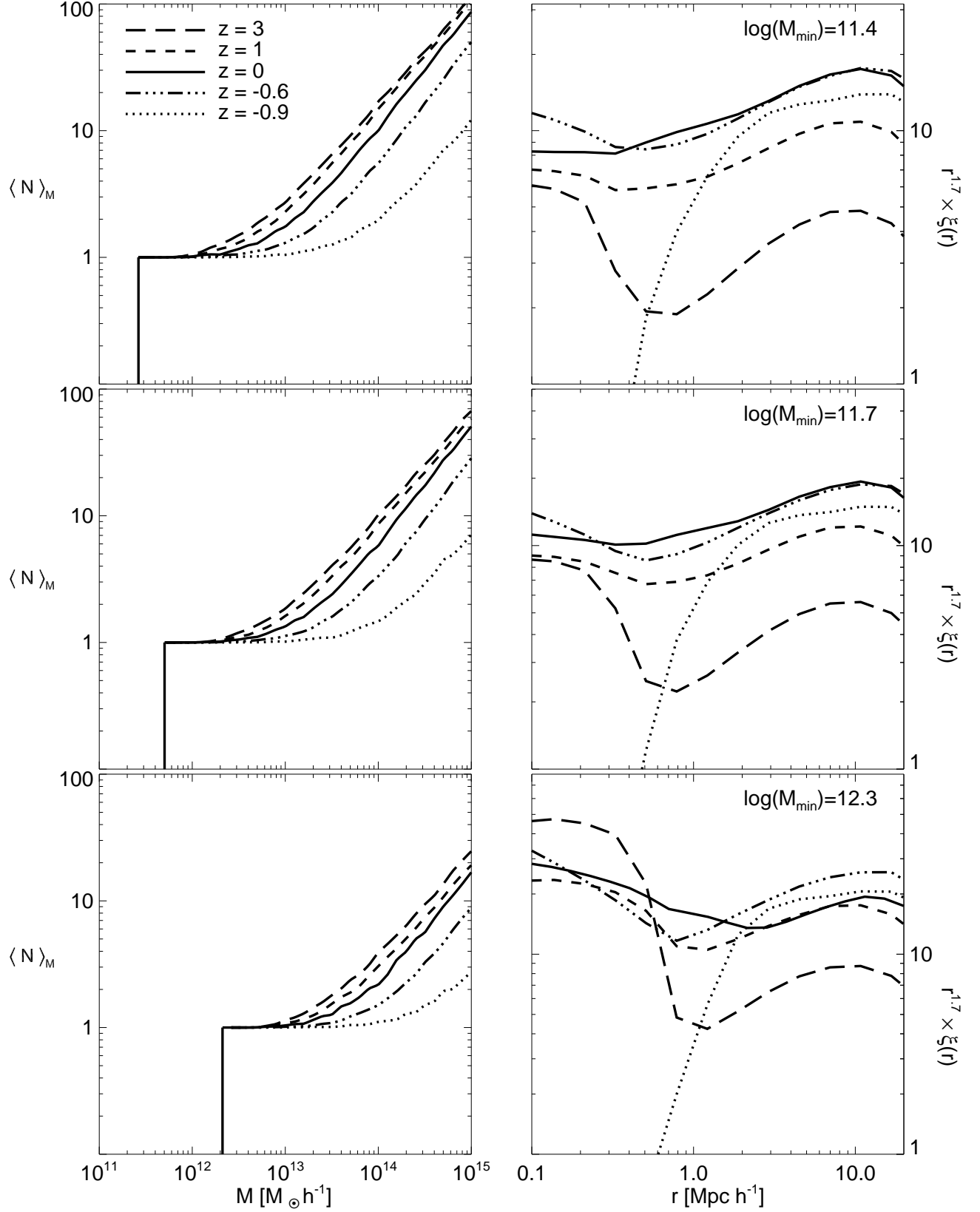
FIG. 4.— *Left panels*: Mean number of all halos (hosts plus subhalos) predicted by our *Full* subhalo model as a function of host halo mass, at five different redshifts. The three panels show results for three mass threshold values: $\log(M_{\mathrm{min}}/h^{-1}M_\odot) = 11.4$, 11.7, and 12.3. The five curves in each panel correspond to the redshifts $z = 3, 1, 0, -0.6, -0.9$ (negative redshifts correspond to future epochs). *Right panels*: Correlation functions corresponding to the halo samples shown in the left panels. In each case, $\xi(r)$ has been scaled by a power law in order to clearly show departures from a power-law shape. The figure shows that the number of subhalos steadily decreases from high to low redshift, causing the correlation function to evolve from not being a power law at high redshift, towards having a nearly power-law shape at the present epoch, and once again deviating from a power law at future epochs.
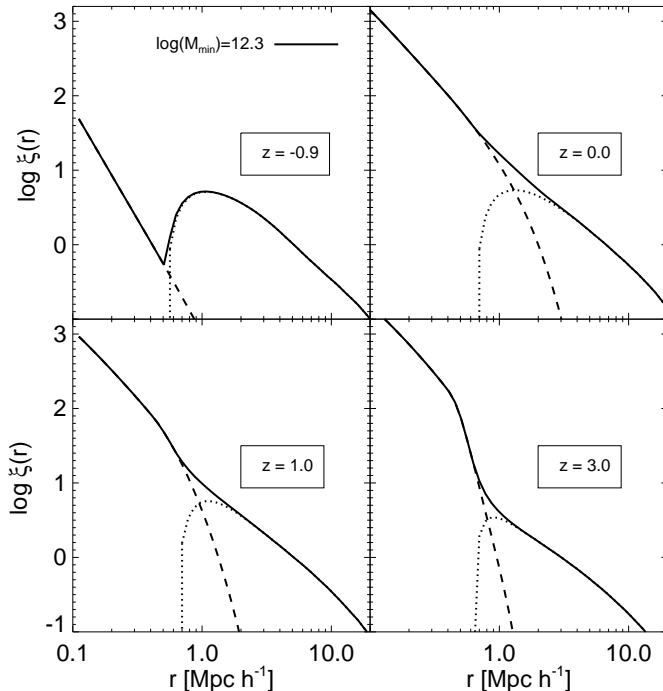
FIG. 5.— The correlation function of all halos (hosts plus subhalos) predicted by our *Full* subhalo model as a function of redshift, for a single mass threshold sample $\log(M_{\mathrm{min}}/h^{-1}M_\odot) = 12.3$. Each panel shows $\xi(r)$ for a different redshift (solid curve), as well as the one-halo (dashed curve) and two-halo (dotted curve) terms. The figure shows that the one-halo term evolves strongly with redshift and only at $z = 0$ strikes the right balance with the two-halo term to result in a power law.

Turning to the right panels, $\xi(r)$ is shown at each redshift scaled by an $r^{-1.7}$ power law in order to emphasize features in the correlation function. Starting at $z = 3$ (long dashed curves), $\xi(r)$ is very far from a power-law, with a slope that is much steeper on small scales. At $z = 1$ (short dashed curves) the break from a power law is less pronounced, but it is still significant. These results are qualitatively consistent with clustering measurements at high redshifts (Coil et al. 2006; Ouchi et al. 2005; Lee et al. 2006). At $z = 0$ (solid curves), the correlation function is approximately a power law, though there is still a mild, discernible feature at the transition scale between the one- and two-halo terms. In the future, $\xi(r)$ once again breaks from a power law. At $z = -0.6$ (dot-dashed curves), departures from a power-law shape are about as strong as they were at $z = 1$. Three Hubble times into the future, at $z = -0.9$ (dotted curves), the departures from a power law are significant and represent a dramatic reduction in the relative contribution of the one-halo term.

Figure 5 focuses on the $\log(M_{\mathrm{min}}/h^{-1}M_\odot) = 12.3$ threshold sample and shows the correlation function at four different redshifts, while also showing the one-halo and two-halo terms explicitly. Figure 5 clearly demonstrates how a delicate balance is needed between the two terms in order for $\xi(r)$ to achieve a power-law shape. The two-halo term exhibits modest variations from panel to panel, with a range of about a factor of ~ 3. The decreased large-scale clustering at $z \gtrsim 0$ is due to the linear growth of perturbations with time, but this is always kept

modest because the increasing bias of halos of fixed mass with redshift (see Zentner 2007) compensates for large-scale structure growth. At $z < 0$, the slight decrease in two-halo clustering is due to the decay of halo bias once halo growth slows (Fry 1996).

The variation in the one-halo term is significantly larger, as our earlier discussions suggest, and changes by a factor of $\sim 45 - 150$ (depending on scale), equivalent to $\sim 15 - 50$ times the variation in the two-halo term. At high redshift, the relative rareness of host halos and the large amount of substructure cause $\xi(r)$ to be boosted significantly in the one-halo regime as shown in the $z = 3$ panel of Figure 5. At $z = 0$, just the right amount of substructure has been depleted to strike a near balance between the one-halo and two-halo contributions. In the future, the continual destruction of subhalos suppresses the one-halo term, driving $\xi(r)$ away from a power law again. By $z = -0.9$, the depression in small-scale clustering is striking.

Some of the evolution of $\xi(r)$ on small-scales comes from the fact that halos large enough to host luminous galaxies become increasingly rare as redshift increases. The characteristic collapsing mass is a rapidly decreasing function of redshift and is only $M_* \approx 10^9 \, h^{-1} \mathrm{M}_\odot$ at $z = 3$. In the relevant regime, the strength of the one-halo term grows in approximate proportion to the number of satellite galaxies and in inverse proportion to the number of host halos of appropriate size (see § 2.1), so the relative paucity of host halos at high redshift also drives strong one-halo clustering because Fig. 5 describes samples of fixed absolute mass threshold. However, it is subhalo abundance that has the larger influence on the redshift dependence of clustering. We have computed the correlations of Figure 5 using samples in which M_{min} varies with redshift so as to maintain a *constant number density* of halos. These samples are less subject to the gross evolution of the halo mass function. We find all of the same qualitative results for this case, though the two-halo term varies by a factor of ~ 4, while the variation in the one-halo term is limited to a factor of $\sim 12 - 80$ (again, depending on scale), resulting in a variation in the one-halo term that is $\sim 3 - 20$ times larger than that of the two-halo term. Moreover, we have re-computed correlation functions using a combination of the predicted low-redshift HODs alongside the high-redshift mass functions in order to isolate the contribution due to the mass function and HOD evolution. The majority the redshift dependence of $\xi(r)$ on small scales is due to the evolution of subhalo abundance. To maintain a power-law correlation function at high-redshift would require fewer subhalos per host than at $z = 0$ in order to compensate for the relative rareness of host halos at high-redshift. In fact, hosts at high redshift have a *larger* number of subhalos of any given mass so these effects *reinforce one another*, leading to a strong deviation from a power-law $\xi(r)$ at high redshift.

We have already described the reasons that the one-halo and two-halo terms behave so differently under changes in the HOD. To reiterate, on large scales, $\xi(r)$ is essentially a weighted average of the clustering of host halos, where $\langle N \rangle_M$ provides the weighting (see the integral in Eqs. [6] and [7], note that $\tilde{\lambda}(k, M) \approx 1$ for $k < 1/R_{\mathrm{vir}}$). The possible variability in $\xi(r)$ on large

scales is limited because it is always bound by the limited variation in the clustering of host halos. As we discussed in § 2.1, the difference in the large-scale bias of the largest relative to the smallest halos is at most a factor of ~ 3 (e.g., Tinker et al. 2005). Significant variations in large-scale clustering require dramatic variations in the HOD at high mass, which are not expected on theoretical grounds and are not mandated by data. However, on scales smaller than the size of individual host halos, $\xi(r)$ can vary dramatically depending on the HOD. For example, in the extreme case of only one object per host halo, there will be zero pairs within halos and the one-halo term will vanish. For large numbers of satellites, the one-halo term will be significantly larger than a power-law extrapolation of the two-halo term to small scales.

The sensitivity of the one-halo term to the HOD, coupled with the relative insensitivity of the two-halo term, means that achieving a power-law correlation function requires fine-tuning in the number of satellite galaxies per halo. The satellite galaxy abundance naturally evolves with redshift, so $\xi(r)$ can only be a power law during those epochs when substructure has evolved to join the one-halo term to the two-halo term. Of course, it may be possible for features in the host halo mass function or bias relations to conspire to compensate for substructure evolution, but such features would somehow need to be coordinated with low-redshift structure growth. A different way to state this is that the halo mass function and halo bias depend on the statistics of the linear density field, and do not "know" about the non-linear galaxy formation and gravitational processes that occur within halos. It would be quite strange if their evolution were somehow connected with the evolution of satellite galaxies in virialized hosts. It seems to be a coincidence that the epoch of near power-law clustering of typical galaxies lies near $z = 0$.

5.3. *The Balance Between Accretion and Destruction*

We have just seen how the depletion of substructure over time leads to evolution in the correlation function such that it becomes a power law at the present epoch. However, what drives substructure depletion? We expect that most subhalos will lose significant amounts of mass or merge with the central galaxy given sufficient time. However, this will be compensated to some degree by the infall of new subhalos. If the rate at which satellites are accreted is greater than the rate at which they are destroyed, then the net amount of substructure will grow with time. The evolution in the number of subhalos (and hence the correlation function) depends on the balance between accretion and destruction. Z05 give a related discussion of accretion and destruction in their § 4.4 and the perspective we adopt here complements Z05.

In Figure 6 we illustrate the competition between accretion and destruction in host halos of mass $M = 10^{13.4}\ h^{-1}\mathrm{M_\odot}$. To measure the accretion rate (dashed curve), we count all subhalos with masses greater than $10^{11}h^{-1}M_\odot$ that accrete onto these hosts in finite time intervals. For the destruction rate (solid curve), we count the number of these same subhalos that drop below $10^{11}h^{-1}M_\odot$ during the time intervals. The accretion rate minus the destruction rate will then give us the net rate of change in the number of subhalos per unit time.

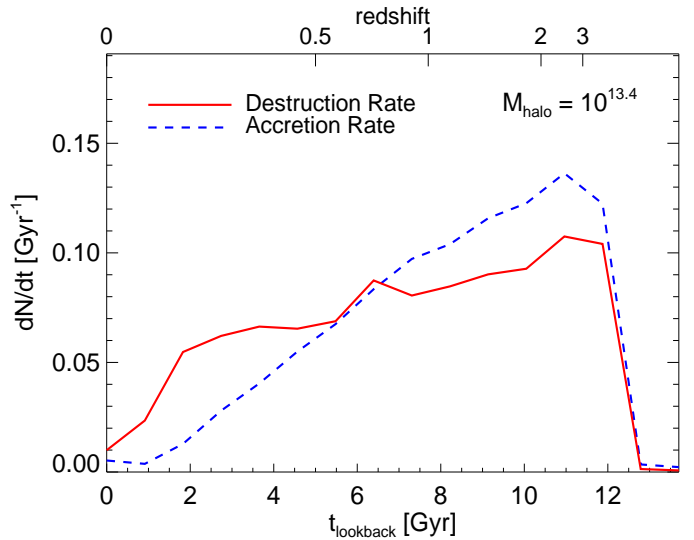Figure 6 shows that the accretion rate quickly grew and

FIG. 6.— The accretion versus destruction rate of subhalos over cosmic time, as predicted by our full subhalo model. The accretion rate shown is the number of subhalos per Gyr that merge into a host halo of mass $\log(M/h^{-1}M_\odot) = 13.4$. The destruction rate is the number of these same subhalos per Gyr that are destroyed (i.e., their mass drops below some threshold value). The two rates equalized when the Universe was $\sim 6\mathrm{Gyr}$ old (at $z \sim 1$). Before $z = 1$, the net number of subhalos increased with time, whereas at later times the net number decreased with time. The figure shows how the balance between accretion and destruction changes with redshift, which explains why the correlation function can only be a power law at a single epoch.

reached a peak at $z \sim 2-3$. Since this peak, the accretion rate has been steadily declining and is close to zero at the present epoch. The decline in merger rates is partly due to the shape of the power spectrum (see Lacey & Cole 1993; Somerville & Kolatt 1999; Zentner 2007), but the driving force for the recent fast decline in the merger rate of halos is the reduced rate of structure growth caused by accelerated cosmic expansion. The destruction rate also peaked at $z \sim 2-3$ and lags the accretion rate because most destruction happens over a period of several dynamical times. Figure 6 clearly shows that the accretion rate has been dropping faster than the destruction rate since their peaks, with accretion and destruction roughly balancing just below $z \sim 1$ (see also Stewart et al. 2009). This means that the number of subhalos in hosts that grow to a mass of $M = 10^{13.4}\ h^{-1}\mathrm{M_\odot}$ by $z = 0$ increased until $z \approx 1$ and has been declining ever since, despite the fact that the virial masses of these halos have been growing. The general trend toward reduced substructure at low redshift explains the behavior exhibited in Figure 4. The correlation function is close to a power law at the present epoch because the balance between accretion and destruction over time has led to the requisite abundance of substructure today.

6. ACHIEVING A POWER-LAW CORRELATION FUNCTION

We now step back from making predictions using our specific subhalo model and undertake a general exploration of the properties of the HOD that yield nearly power-law correlation functions at different masses and redshifts. The HOD characterizes the number and spatial distribution of galaxies within dark matter halos. It is typically specified with a handful of parameters that

are constrained using galaxy clustering measurements (e.g., Magliocchetti & Porciani 2003; Zehavi et al. 2005; Tinker et al. 2005; Zheng et al. 2007). We choose an HOD model that is motivated by theoretical predictions from hydrodynamic simulations, semi-analytic models, and high-resolution N-body simulations (Berlind et al. 2003; Kravtsov et al. 2004a; Zheng et al. 2005). According to this model, halos above some threshold mass contain a single "central" galaxy plus a number of "satellite" galaxies. The number of satellites in any given halo is drawn from a Poisson distribution whose mean is a power-law function of host halo mass. The central galaxy is placed at the center of the host halo, while the satellites are spatially distributed according to an NFW density profile. Specifically, we adopt an HOD parametrization that is similar to the one used by Tinker et al. (2005). This is a simple, yet powerful model in which the number of central galaxies is modeled as a step function,

$$N_{\rm cen} = \begin{cases} 1 & \text{if } M \geq M_{\rm min} \\ 0 & \text{if } M < M_{\rm min} \end{cases} , \qquad (8)$$

while the mean number of satellites follows a power-law with an exponential cutoff at low mass,

$$\langle N_{\rm sat} \rangle_M = \left(\frac{M}{M_1} \right)^\alpha \exp\left(\frac{-M_0}{M} \right). \qquad (9)$$

The parameters in the model are as follows.

1. $M_{\rm min}$ is the minimum host halo mass to contain a central galaxy.

2. M_0 is the host halo mass below which satellite galaxies are exponentially supressed.

3. M_1 is the host halo mass to contain, on average, one satellite galaxy.

4. α is the index of the power-law relation between the mean number of satellite galaxies and halo mass.

Previous studies have shown that the power-law index $\alpha \approx 1$ for subhalos and simulated galaxies (Kravtsov et al. 2004a; Zheng et al. 2005; Zentner et al. 2005), as well as observed galaxies dimmer than L_* (Zehavi et al. 2005), leading Tinker et al. (2005) to set $\alpha = 1$ throughout their analysis. However, we allow α to vary because the correlation function is sensitive to it and, although it may be near unity when modeling observed data, it may need to deviate from unity to yield a power-law correlation function at high redshifts. On the other hand, $\xi(r)$ is not sensitive to M_0, consequently we fix its value by adopting the Conroy et al. (2006) $M_0 - M_1$ relation,

$$\log(M_0/h^{-1}M_\odot) = 0.76 \log(M_1/h^{-1}M_\odot) + 2.3. \quad (10)$$

The result is an HOD model with only three free parameters: $M_{\rm min}$, M_1, and α.

The two-halo term of $\xi(r)$ depends on the mean occupation $\langle N \rangle_M = \langle N_{\rm cen} + N_{\rm sat} \rangle_M$, which is equal to $1 + \langle N_{\rm sat} \rangle_M$ for $M > M_{\rm min}$. The one-halo term also requires the second moment of the occupation distribution $\langle N_{\rm sat}(N_{\rm sat} - 1) \rangle_M$, so characterizing the mean occupation is not sufficient. We assume that the number of satellites follows a Poisson distribution, for which

$\langle N_{\rm sat}(N_{\rm sat} - 1) \rangle_M \equiv \langle N_{\rm sat} \rangle_M^2$. Our *Full* model deviates mildly from a pure Poisson distribution (see Fig. 7 of Z05, and recent simulations of Boylan-Kolchin et al. 2010, that find similar deviations from a Poisson distribution), but the effect of this deviation on $\xi(r)$ is minor (Fig. 16 of Z05). We also note that there are any number of possible parametrizations for $\langle N_{\rm sat} \rangle_M$ to choose from besides the one adopted here. We have found that mildly different parametrizations that exhibit the same basic features and are consistent with contemporary data (e.g., the one used by Zehavi et al. 2005) yield similar conclusions.

We consider the HOD parameter space that yields a power-law correlation function for three galaxy samples of fixed number density $\bar{n}_{\rm g}$, at three different redshifts $z = 0, 1, 3$. Fixing number density is a way to compare similar samples at different redshifts because the high-redshift sample is more likely to represent the progenitors of the low-redshift sample than it would in the case of mass threshold samples. We choose number densities equal to $\bar{n}_{\rm g} = 0.02$, 0.01, and 0.003 $h^3{\rm Mpc}^{-3}$, which correspond to three $z \simeq 0$, volume-limited, r-band threshold samples in the SDSS: $M_r < -18.5$, -19.5, and -20.5 (Zehavi et al. 2005).

For a given number density and redshift combination (e.g., $\bar{n}_{\rm g} = 0.02 \ h^3{\rm Mpc}^{-3}$ at $z = 1$), we create a 50×50 grid of $M_1 - \alpha$ parameter combinations. For each pair of M_1 and α on this grid, we use Equation (3) to find the value of $M_{\rm min}$ that is needed to enforce the desired number density. In this manner, the 2,500 HOD models on the grid represent galaxy samples with the same number densities, but different HODs. We then compute the first and second moments of the mean galaxy occupation using equations (8) and (9), and use the halo model described in § 2.1 to construct $\xi(r)$. We assign 10% errors on all scales to $\xi(r)$, as such errors are roughly consistent with jackknife re-sampling errors in current clustering measurements (Zehavi et al. 2005), and we fit a power-law function to all 2,500 correlation functions. We perform our fits using a Markov Chain Monte Carlo (MCMC) analysis in which we vary the slope and correlation length of the fitted power-law. We then find the minimum χ^2 value for a power-law fit to $\xi(r)$ for any given $M_1 - \alpha$ combination. This allows us to approximate the HOD parameter space in which $\xi(r)$ is consistent with a power law at a level similar to contemporary observations. For two free parameters, the 68.3% (1σ), 95% (2σ), and 99.6% (3σ) likelihood regions correspond to values of reduced $\chi^2 \leq 1.15$, 1.61, and 2.06, respectively.

Figure 7 shows the contours generated from the aforementioned procedure. Each row in the figure represents a different $\bar{n}_{\rm g}$ value and each column corresponds to a different redshift. The "satellite fraction" ($f_{\rm sat}$, the fraction of all galaxies that are satellites, see Eq. [5]) is relevant to the shape of the galaxy two-point correlation function. Therefore, over-plotted in each panel are curves of constant $f_{\rm sat}$ (the labeled, solid, black curves). To compare these results with measurements from observed galaxies, in each panel we also show best-fit M_1 and α values from published halo model fits to measurements of $\xi(r)$ using galaxy samples with the same number densities at the same redshifts. Squares and
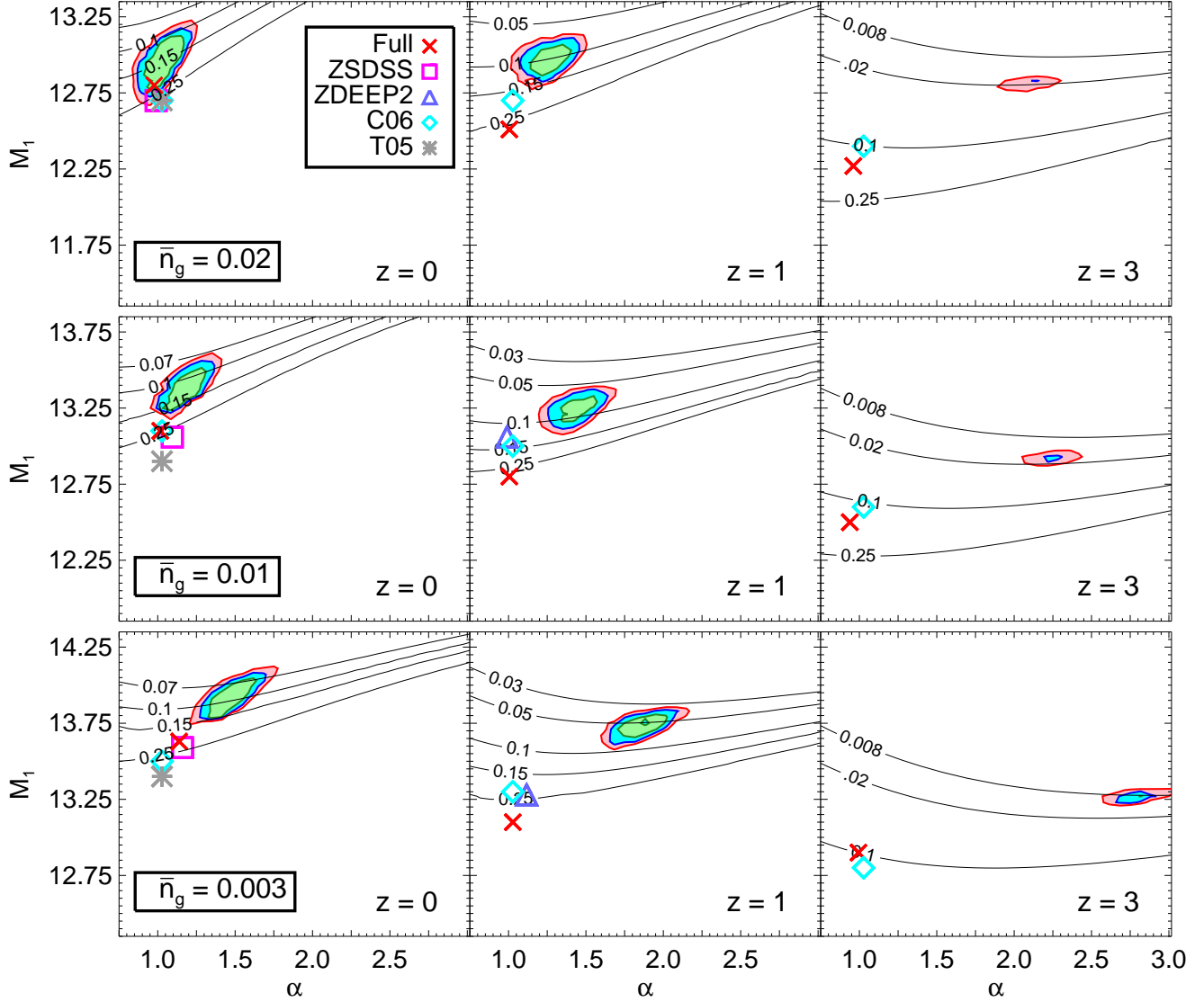
FIG. 7.— Exploration of the HOD parameter space that yields a power-law $\xi(r)$, as a function of redshift and sample number density. Each column of panels shows results for a different redshift ($z = 0, 1, 3$). Each row of panels shows results for a different sample number density ($\bar{n}_g = 0.02, 0.01, 0.003h^3\text{Mpc}^{-3}$). We adopt the four-parameter HOD model shown in equations 8, 9, and 10. Each panel shows the parameter space probed by α, the slope of the mean occupation number of satellites, and M_1, the halo mass that contains on average one satellite galaxy. For each pair of α and M_1 values, we find the value of M_{min} that yields the desired galaxy number density. We then use the halo model to compute $\xi(r)$ for that set of HOD parameters. We do this on a 50×50 grid of $\alpha - M_1$ parameter combinations. We fit each correlation function to a power law, and the shaded contours represent the 68.3%, 95% and 99.6% power-law likelihood (green, blue, red contours). Also shown are contours of constant satellite fraction (solid black curves). The red X in each panel shows the HOD parameters predicted by our *Full* subhalo model. For comparison, we also show results from HOD modeling of real galaxy samples from the SDSS at $z = 0$ (Zheng et al. 2007, T05 - magenta boxes and grey asterisks); and DEEP2 at $z = 1$ (Zheng et al. 2007 - purple triangles). Finally, we show the simulation results of Conroy et al. (2006) that are designed to model SDSS, DEEP2, and Lyman-break galaxies at $z = 0, 1$, and 3, respectively (cyan diamonds).

triangles represent the best-fit parameter values from Zheng et al. (2007) who fit SDSS ($z = 0$) and DEEP2 ($z = 1$) data (ZSDSS, ZDEEP2) and asterisks represent the best-fit Tinker et al. (2005) values for SDSS data (T05). Diamonds represent the Conroy et al. (2006) values for SDSS, DEEP2, and the $z = 3$ Subaru data of Lyman-break galaxies (C06).

The best-fit parameter combinations should be regarded as best-fit "regions", because there are errors associated with the derived parameters (e.g., the

Zheng et al. (2007) SDSS α and M_1 errors at each luminosity are of order 10%). We note that Tinker et al. (2005) considered several possible values of σ_8, but we show their results for $\sigma_8 = 0.9$ to be consistent with the cosmological model used in the other studies. Finally, in each panel we show the HOD parameters predicted by our *Full* subhalo model (marked by an "X") for samples with mass thresholds that yield the desired number density. The *Full* model gives $\langle N_{\text{sat}} \rangle_M$ and we fit this with Equation (9) to obtain best-fit values of M_1 and α.

Several interesting conclusions can be drawn from this figure.

1. The region of HOD parameter space that yields a power-law $\xi(r)$ drifts to lower values of both M_1 and α with increasing number density. These trends increase the satellite fraction as number density increases to compensate for the relative reduction in the one-halo term compared to the two-halo term induced by moving to a lower-mass, more abundant halo sample.

2. The values of α that result in the best power laws drift higher with increasing redshift in an effort to boost the two-halo term by placing galaxies in massive, highly-biased halos. In general, it is difficult to arrange a power law at $z \geq 3$ for these three number densities.

3. As might be expected from our previous discussions, there is a relatively narrow range of $f_{\rm sat}$ for the best-fit power-law space at each redshift. At $z = 0$, the space that is consistent with a power-law with 10% errors on the data lie near $f_{\rm sat} \sim 0.1 - 0.15$. The direct fits to observational data lie near $f_{\rm sat} = 0.2 - 0.3$. At $z = 1$, the power-law region is shifted to $f_{\rm sat} \sim 0.05 - 0.1$, while at $z = 3$ the power-law region is even lower, $f_{\rm sat} \sim 0.01 - 0.02$. Note that the power-law regions are not precisely aligned along constant-$f_{\rm sat}$ contours, particularly at low redshift and low number density, indicating that other factors, such as host halo abundances and the physical sizes of host halos, contribute to the power-law nature of $\xi(r)$. However, at high redshift and low number density, the power-law regions become more nearly co-linear with contours of constant $f_{\rm sat}$ over a range of α values.

4. The SDSS ($z \sim 0$) best-fit points lie near the power-law contours, but not within these likelihood regions. This is not surprising as the SDSS measurement is more precise over a wide range of scales than the $\sim 10\%$ errors we have assumed and the observed $\xi(r)$ is now known to exhibit very small, but statistically-significant deviations from a power law (Zehavi et al. 2004).

5. As predicted from Figure 3, the fits to observational data lie further from the power-law regions as we move to lower $\bar{n}_{\rm g}$ (higher luminosity) samples. At fixed redshift, this is driven largely because the host halos of these galaxies become increasingly rare. However, it is worth noting that the growth of the one-halo term with increasing $M_{\rm min}$ is reinforced by an increase in satellite abundance at fixed scaled mass $M_{\rm sub}/M_{\rm host}$ as $M_{\rm host}$ increases, accounting for $\sim 30\%$ of the rise. This increase satellite abundance with $M_{\rm host}$ arises because more massive host halos assemble more recently, leaving less time for the evolution of substructure and less satellite destruction (Z05). The relative time available for satellite evolution is an important part of determining the power-law nature of the correlation function.

6. The fits to observational data lie near the power-law regions at $z = 0$, but grow more distinctly separated with increasing redshift. This evolution is driven by satellite fractions at high-z that are too large to be consistent with power-law clustering. This supports our basic picture that satellite destruction over cosmic time is needed to achieve a power law $\xi(r)$, and that the observed low-luminosity, low-redshift $\xi(r)$ is a coincidence.

7. The HOD values predicted by our *Full* subhalo model are similar to all of the observed data fits at all redshifts. This is a remarkable result considering our model treats only subhalos and not galaxies explicitly. We explore more complicated associations of galaxies and subhalos in a follow-up study.

8. Our subhalos, as well as all observational data, reveal values of $\alpha \simeq 1$ for all redshifts, in accord with previous theoretical results (Kravtsov et al. 2004a; Zheng et al. 2005; Zentner et al. 2005; Conroy et al. 2006). Moreover, at each redshift, they have fixed satellite fractions, independent of $\bar{n}_{\rm g}$. At $z = 0$, $z = 1$, and $z = 3$, our model and the observational data cluster near $f_{\rm sat} \approx 0.25$, $f_{\rm sat} \approx 0.2$, and $f_{\rm sat} \approx 0.1$, respectively. We note that the lower satellite fractions at high redshift are *not* due to HOD evolution. Figure 4 shows that $\langle N_{\rm sat} \rangle$ is higher at high z. Instead, satellite fractions are lower at high z because all relevant host halos have $M_{\rm host} > M_*$ and lie on the exponentially-decreasing portion of the halo mass function, so the relative number of M_1-mass host halos to $M_{\rm min}$-mass halos decreases with redshift. Nevertheless, these satellite fractions at high redshift are too high to support a power-law galaxy correlation function.

9. Figure 7 implies that the physical mechanisms that dictate the HOD of galaxies operate to maintain α and $f_{\rm sat}$ approximately fixed and *not* to achieve a power-law correlation function.

We have established that the observed power-law correlation function at low masses and low redshifts should not persist at higher masses or redshifts for simple, physical reasons. However, exploring the HOD parameter space has not revealed a single simple property that yields a power-law shape for $\xi(r)$. In an effort to better understand the factors that drive a power-law $\xi(r)$ at high precision, we continue to explore the HOD parameter space in a different way. Specifically, we investigate the two mass scales in the standard HOD models, $M_{\rm min}$ and M_1, relative to the characteristic non-linear collapse mass, M_*. To complement our previous analysis and to be consistent with gross theoretical predictions, we fix $\alpha = 1$ and take our two parameters to be $M_{\rm min}/M_*$ and $M_1/M_{\rm min}$. The first ratio specifies roughly the host masses that galaxies occupy relative to the exponential regime of the halo mass function, and the second ratio sets the length of the "plateau" in the HOD.

Figure 8 probes the power-law $\xi(r)$ space as a function of the ratios $M_{\rm min}/M_*$ and $M_1/M_{\rm min}$. For this analysis we switch from fixed number density samples to
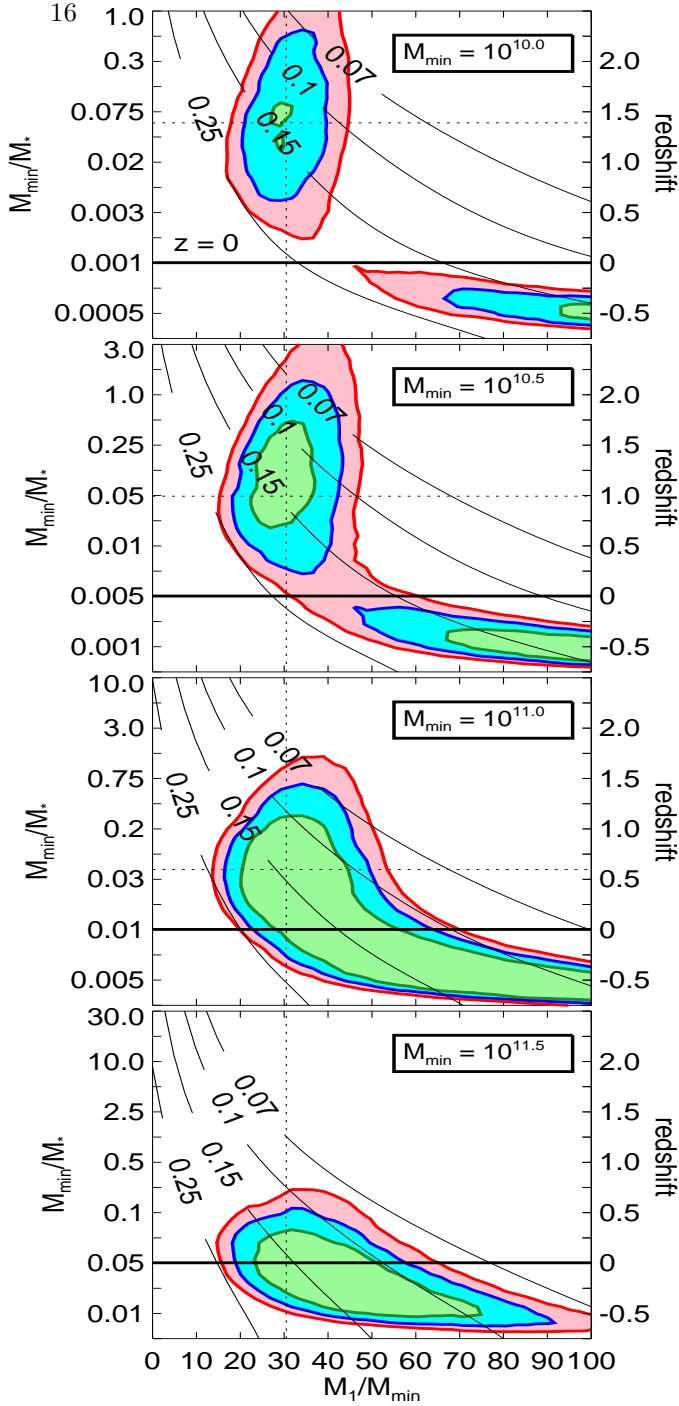
FIG. 8.— Exploration of the HOD parameter space that yields a power-law $\xi(r)$. Each panel corresponds to a different mass threshold $M_{\min}$ (in units of $h^{-1}M_\odot$). The y-axis shows redshift (right-hand side), which also corresponds directly to the ratio $M_{\min}/M_*$ (left-hand side), since the characteristic non-linear mass M_* depends directly on redshift. The horizontal axis shows the ratio $M_1/M_{\min}$. We fix the slope of the satellite mean occupation function to be $\alpha = 1$ and we set the fourth HOD parameter M_0 using equation 10. Each point on the horizontal axis therefore corresponds to a specific set of HOD parameters, while moving along the vertical axis shifts the HOD to different redshifts. As in Fig. 7, shaded contours represent the 68.3%, 95% and 99.6% power-law likelihood spaces and thin solid curves show contours of constant satellite fraction. The horizontal and vertical dotted lines correspond to fixed values of $M_{\min}/M_* = 0.05$ and $M_1/M_{\min} = 30$, which bisect the best-fit power-law space in all four panels. Solid black horizontal lines denote $z = 0$, below which the parameter space corresponds to future epochs.

fixed mass thresholds, and we choose four values of minimum mass that correspond to a range of sub-L_* galaxies ($M_{\min} = 10^{10.0}, 10^{10.5}, 10^{11.0}, 10^{11.5}h^{-1}M_\odot$), showing results for each in a distinct panel. In each panel, we sample redshifts from $z = -0.9$ to $z = 2.9$ in steps of $\Delta z = 0.08$ (labeled on the right vertical axis). Each redshift value also corresponds to a $M_{\min}/M_*$ ratio, which we label on the left vertical axis. At each redshift, we also loop over $M_1/M_{\min}$ ratios from 1 to 100 in steps of $\Delta(M_1/M_{\min}) = 2$. For every pair of $M_{\min}/M_*$ and $M_1/M_{\min}$ values, we compute $\xi(r)$ using the halo model and fit a power-law function in the same fashion as described previously. As before, we show the 68.3%, 95% and 99.6% likelihood regions of $\xi(r)$ consistent with a power law (green, blue, and red contours, respectively). Also, as before, we show contours of constant satellite fraction, $f_{\rm sat}$ (solid black curves). The thick horizontal lines at $z = 0$ are meant to emphasize that the parameter space lying below these lines corresponds to *future* epochs.

We have repeated this analysis for higher mass thresholds (values of $M_{\min} = 10^{12.0}, 10^{12.5}, 10^{13.0}, 10^{13.5}h^{-1}M_\odot$). However, we do not show those results because we found no parameter combinations within the 99.6% power-law likelihood space. Figure 7 showed that the power-law parameter space drifted to higher values of α for lower number density (and hence higher mass) samples in an effort to drive up the two-halo term to meet the enhanced one-halo term. Therefore, it is not surprising that we do not find this space when we restrict the slope to be $\alpha = 1$.

Many interesting results can be drawn from Figure 8. Again, we itemize them for the sake of clarity.

1. In order for $\xi(r)$ to have a shape consistent with a power-law assuming $\sim 10\%$ measurement errors, it appears necessary for the "plateau" in the HOD to be sufficiently long. At all masses and redshifts, $M_1/M_{\min}$ needs to be at least ~ 20, otherwise the large satellite fraction drives a one-halo term that is too large relative to the two-halo term. Moreover, for past epochs, $z > 0$, the maximum plateau length is $M_1/M_{\min} \lesssim 40$. Higher values of $M_1/M_{\min}$ yield a one-halo term that is too weak. In fact, $M_1/M_{\min} \sim 30$ seems to be the preferred value to yield a nearly power-law correlation function at all masses so long as $z > 0$. This value is denoted by the vertical dotted lines in all the panels.

2. For $z \geq 0$, a near power-law $\xi(r)$ seems to require a restricted range of $M_{\min}/M_*$. Interestingly, the value $M_{\min}/M_* \sim 0.05$ can yield a power-law correlation function at all masses for appropriate choices of redshift. This value is denoted by the horizontal dotted lines in all the panels. This restriction on $M_{\min}/M_*$ means that higher redshift samples (when M_* is significantly smaller than today) can only exhibit power-law behavior if the relevant host halos are significantly smaller. This possibility becomes irrelevant in a practical sense because star formation is inefficient in small halos ($M \ll 10^{11}h^{-1}M_\odot$, e.g., Conroy & Wechsler 2009; Behroozi et al. 2010; Guo et al. 2010)), so

they cannot host galaxies that are easily observable at high redshift. Figure 8 shows that the lowest-mass samples that we consider (top two panels) have a nearly power-law $\xi(r)$ at $1 \lesssim z \lesssim 2$, whereas the highest-mass samples have a nearly power-law $\xi(r)$ only at low redshift.

3. At sufficiently high redshift, near power-law clustering is no longer achievable at any mass threshold corresponding to relatively bright galaxies. Our results generally indicate that power-law clustering at high redshift can only be achieved if galaxies at high redshift occupy halos in a markedly different and more complicated manner than their low-z counterparts.

4. For future epochs these broad results no longer hold. A broader range of $M_1/M_{\rm min}$ values can be made approximately consistent with a power law at low values of $M_{\rm min}/M_*$, or low/negative redshifts. For the lowest $M_{\rm min}$ samples the power-law likelihood space is clearly bimodal, with possible ways to achieve a power law both at high redshifts and at low/future redshifts.

5. At all masses and redshifts we find that the power-law likelihood parameter space has satellite fractions in the range $f_{\rm sat} \sim 0.1 - 0.25$, with the $f_{\rm sat} = 0.15$ contour slicing through all of the 1σ regions. $f_{\rm sat}$ is naturally strongly dependent on both $M_1/M_{\rm min}$ and $M_{\rm min}/M_*$. Increasing the length of the HOD plateau at fixed $M_{\rm min}$ and redshift makes $f_{\rm sat}$ decrease, as does boosting $M_{\rm min}/M_*$ while keeping $M_{\rm min}$ and the plateau fixed. If we keep both ratios fixed (i.e., both the HOD shape and its position relative to the mass function) then the satellite fraction is also approximately fixed, regardless of $M_{\rm min}$.

7. DISCUSSION AND PRIMARY CONCLUSIONS

It has been recognized for decades that the two-point correlation function has a simple, power-law form with $\xi(r) \sim r^{-2}$. Observational determinations of galaxy two-point clustering spanning more than thirty years all yielded results consistent with a single power law extending from linear and quasi-linear length scales ($r \gtrsim 30\,h^{-1}{\rm Mpc}$) to deeply non-linear scales ($r \lesssim 0.1\,h^{-1}{\rm Mpc}$). In this paper, we cast the problem in the contemporary setting in which galaxies form in halos and subhalos of dark matter and set out to understand the physical processes that drive this surprisingly simple result. Our primary conclusion is that the nearly power-law correlation function of relatively common, L_* and sub-L_* Galaxies at $z \sim 0$ is a coincidence and does not reflect any general principle of structure formation or galaxy evolution. So how did we arrive at this conclusion?

First, the efficiency of galaxy formation is dependent upon halo mass and it has been determined both theoretically and empirically that there is a halo mass scale below which galaxy formation is inefficient, roughly $M_{\rm gal} \sim 10^{10.5}\,h^{-1}M_\odot$ (Conroy & Wechsler 2009; Behroozi et al. 2010; Guo et al. 2010). A number of things can set this scale including atomic and molecular physics and feedback from supernovae and active galactic nuclei (for a recent review article see Benson 2010). This mass scale is $M_{\rm gal} < M_*$, so L_* and sub-L_* galaxies are common. Had $M_{\rm gal}$ been greater than or similar to M_*, most bright galaxies would lie in comparably rare halos and be rare themselves. In such a case, one-halo clustering would be too strong to be compatible with a power law. M_* is *not* determined by galaxy formation physics but is set by the completely unrelated processes that establish the amplitude of cosmological density fluctuations, presumably primordial inflation.

Second, power-law clustering requires that some of the galaxies formed within relatively large subhalos are destroyed. Destruction is due primarily to mass loss, and, to a lesser extent, merging with the central galaxy as a result of dynamical friction. Without this destruction, satellite fractions would be too high and small-scale clustering too strong compared with large-scale clustering. In a forthcoming paper, we perform more sophisticated modeling to make the connection between subhalo mass loss and stellar mass loss in order to make predictions for the amount of intracluster light. Large-scale clustering is principally set by large-scale matter density fluctuations and is insensitive to the details of galaxy formation within halos, while the strength of small scale clustering grows in proportion to the fraction of galaxies that are satellites and in inverse proportion to the number density of the galaxies of interest. As it turns out, precisely the right amount of subhalo destruction has occurred by redshift $z \sim 0$ in a concordance cosmology to produce a single, unbroken, power-law $\xi(r)$.

Evolution of the satellite fraction is set by a competition between halo mergers, which increase $f_{\rm sat}$, and destruction by dynamical processes, which occur on a dynamical timescale and reduce $f_{\rm sat}$. At high redshifts, mergers occur more rapidly than destruction for halos with masses $\gtrsim M_{\rm gal}$. The low-redshift merger rate declines in part due to the fact that $M_{\rm gal} < M_*$ at $z \lesssim 1$. Halos with masses below M_* become relatively more likely to merge with a larger object than to acquire new substructure compared to counterparts with masses greater than M_* (see Zentner 2007). More importantly, the rate of halo mergers is quenched at $z \lesssim 1$ as dark energy begins to suppress further cosmological structure growth. As merger rates decline, satellites are depleted with time. Therefore, at $z \sim 0$, the correlation function is nearly a power law because the competition between the accretion and destruction rates has struck just the right balance to yield the appropriate value of $f_{\rm sat}$.

The merger and destruction rates will once again become unbalanced in the future as halo merging is stifled by dark energy and existing satellite galaxies are slowly destroyed over many dynamical times through complex interactions in their host environments. We show that this will result in small-scale clustering that will be significantly *too weak* to be consistent with a power law.

Largely as a consequence of the merger/destruction competition, $\xi(r)$ evolves through cosmic time, achieving a power law only near $z \sim 0$ for $L \sim L_*$ and dimmer galaxies. The processes of galaxy formation, the amplitude of cosmological density fluctuations, the abundance of dark matter, and the nature of the dark energy are thought to be completely distinct and determined by *unrelated physics*. So the power-law $\xi(r)$ at $z \sim 0$ is a coincidental conspiracy.

In establishing these broad conclusions, we have performed an exhaustive investigation of the ingredients of the galaxy correlation function, which has revealed many interesting, more detailed conclusions. These can be summarized as follows.

1. We find that satellite halo mass loss is the principle dynamical process responsible for depleting sufficient substructure so as to nearly align the one- and two-halo terms to yield a power-law correlation function at low redshift. Dynamical friction plays a smaller supporting role, accounting for an additional $\sim 15\%$ of subhalo destruction.

2. The shape of the correlation function is strongly mass dependent. For instance, at low redshift deviations from a power law $\xi(r)$ grow with increasing host halo mass. This drives stronger deviations from a power law for higher luminosity galaxy samples. The best power-law fits derived from our model are for galaxies residing in halos that are common enough to correspond to $\sim L_*$ and dimmer galaxies, in agreement with observations.

3. The correlation function is highly redshift-dependent. The sensitivity of the one-halo term to the HOD, coupled with the relative insensitivity of the two-halo term, implies that achieving a power-law requires fine-tuning the number of satellite galaxies per halo. The satellite galaxy abundance evolves with redshift, driven by the evolving balance between accretion and destruction, with an enhanced amount of substructure at high redshift. Therefore, the correlation function can only achieve a power law during those epochs when substructure has evolved to align the one- and two-halo terms. The correlation function is boosted on small scales at high z, the one- and two-halo terms join at $z = 0$ to form a power-law, then the power law is once again broken in future epochs.

4. For three chosen number densities corresponding to low-redshift, $\sim L_*$ and dimmer galaxies, we probed the most likely power-law space as a function of redshift for a parametrized HOD. We find that there is a relatively narrow range of satellite fractions for $\xi(r)$ to be consistent with a single power law (assuming $\sim 10\%$ measurement errors) at any given redshift. At all redshifts and masses, power-law correlation functions have satellite fractions in the range $f_{\rm sat} \sim 0.1 - 0.25$. It is difficult to achieve a power-law correlation function at $z \gtrsim 3$ for any number density.

5. We find that to achieve a power law $\xi(r)$ at high mass or redshift, the slope α of the satellite galaxy occupation function must be significantly steeper than unity (for instance, greater than 2 at $z = 3$). This would imply that the mapping of galaxies to halos is much more complicated than we think,

since the number of galaxies would have to be very different than the number of subhalos of a particular size. Instead, it appears that the processes that govern galaxy formation do not care about the conditions needed to achieve a power law $\xi(r)$.

6. The ratio $M_1/M_{\rm min}$ (the "plateau" of the HOD) is a key ingredient for predicting the shape of $\xi(r)$. The prominence of the plateau is a measure of substructure abundance. Along with $M_1/M_{\rm min}$, it is also necessary to characterize the ratio $M_{\rm min}/M_*$, which specifies what halo masses galaxies occupy relative to the halo mass function. By maintaining the combination of $M_1/M_{\rm min} \sim 30$ and $M_{\rm min}/M_* \sim 0.05$ we can achieve a near power law for redshifts in the range $0 - 1.5$ and the appropriate mass threshold at each redshift (the mass threshold is $M_{\rm min} \sim M_*/20$, with M_* set by the redshift). At higher redshifts this criterion is met for galaxies that are most likely too dim to be observed. For example, achieving the requisite $M_{\rm min} \sim M_*/20$ at $z = 2$ corresponds to a halo mass of $M_{\rm min} \sim 10^9\, h^{-1} M_\odot$ in which star formation is inefficient.

This work has allowed us to formulate a general picture of the nature of the galaxy two-point correlation function. Halo abundances and subhalo populations evolve with time. At high redshifts, halos large enough to harbor galaxies are rare and subhalos are abundant within these hosts. With time, host halos that harbor galaxies generally become more common (though the specifics of this evolution can be subtle) and subhalos within these hosts become relatively less abundant. All the while, large-scale matter correlations grow, but the clustering bias of large halos evolves to largely compensate for this large-scale growth of structure. These effects, considered either individually or in tandem, change the HOD and the shape of $\xi(r)$. As a result, the correlation function evolves through an epoch where it is close to a power law and this epoch happens to be near $z \sim 0$. From our broad discussion and detailed conclusions, it is clear that a nearly power-law correlation function requires a conspiracy between otherwise unrelated processes such as the early Universe physics that established the initial conditions for low redshift structure, the detailed physical processes that determine galaxy and star formation efficiency, and the growth rate of cosmic structure set largely by the abundances of dark matter and dark energy. The low-redshift power-law galaxy two-point function is thus a mere cosmic coincidence.

REFERENCES

Baugh, C. M. 1996, MNRAS, 280, 267
Behroozi, P. S., Conroy, C., & Wechsler, R. H. 2010, ApJ, 717, 379
Benson, A. J. 2005, MNRAS, 358, 551
——. 2010, Phys. Rep., 495, 33
Berlind, A. A., & Weinberg, D. H. 2002, ApJ, 575, 587
Berlind, A. A., et al. 2003, ApJ, 593, 1

Binney, J., & Tremaine, S. 2008, Galactic Dynamics: Second Edition (Princeton University Press)

Blake, C., Collister, A., & Lahav, O. 2008, MNRAS, 385, 1257

Blumenthal, G. R., Faber, S. M., Primack, J. R., & Rees, M. J. 1984, Nature, 311, 517

Bond, J. R., Cole, S., Efstathiou, G., & Kaiser, N. 1991, ApJ, 379, 440

Boylan-Kolchin, M., Springel, V., White, S. D. M., & Jenkins, A. 2010, MNRAS, 406, 896

Busha, M. T., Wechsler, R. H., Behroozi, P. S., Gerke, B. F., Klypin, A. A., & Primack, J. R. 2010, ArXiv e-prints

Carroll, S. M., Press, W. H., & Turner, E. L. 1992, ARA&A, 30, 499

Chandrasekhar, S. 1943, ApJ, 97, 255

Coil, A. L., Newman, J. A., Cooper, M. C., Davis, M., Faber, S. M., Koo, D. C., & Willmer, C. N. A. 2006, ApJ, 644, 671

Colín, P., Klypin, A. A., Kravtsov, A. V., & Khokhlov, A. M. 1999, ApJ, 523, 32

Colless, M., et al. 2001, MNRAS, 328, 1039

Conroy, C., & Wechsler, R. H. 2009, ApJ, 696, 620

Conroy, C., Wechsler, R. H., & Kravtsov, A. V. 2006, ApJ, 647, 201

Cooray, A., & Sheth, R. 2002, Phys. Rep., 372, 1

da Costa, L. N., et al. 1988, ApJ, 327, 544

de Lapparent, V., Geller, M. J., & Huchra, J. P. 1988, ApJ, 332, 44

Faltenbacher, A., & Mathews, W. G. 2005, MNRAS, 362, 498

Fry, J. N. 1996, ApJ, 461, L65+

Ghigna, S., Moore, B., Governato, F., Lake, G., Quinn, T., & Stadel, J. 1998, MNRAS, 300, 146

Giocoli, C., Pieri, L., Tormen, G., & Moreno, J. 2009, MNRAS, 395, 1620

Giocoli, C., Tormen, G., & van den Bosch, F. C. 2008, MNRAS, 386, 2135

Gott, III, J. R., & Turner, E. L. 1979, ApJ, 232, L79

Guo, Q., White, S., Li, C., & Boylan-Kolchin, M. 2010, MNRAS, 404, 1111

Hamilton, A. J. S., & Tegmark, M. 2002, MNRAS, 330, 506

Hashimoto, Y., Funato, Y., & Makino, J. 2003, ApJ, 582, 196

Hauser, M. G., & Peebles, P. J. E. 1973, ApJ, 185, 757

Hayashi, E., Navarro, J. F., Taylor, J. E., Stadel, J., & Quinn, T. 2003, ApJ, 584, 541

Hermit, S., Santiago, B. X., Lahav, O., Strauss, M. A., Davis, M., Dressler, A., & Huchra, J. P. 1996, MNRAS, 283, 709

Huchra, J., Davis, M., Latham, D., & Tonry, J. 1983, ApJS, 52, 89

Jenkins, A., et al. 1998, ApJ, 499, 20

Jenkins, A., Frenk, C. S., White, S. D. M., Colberg, J. M., Cole, S., Evrard, A. E., Couchman, H. M. P., & Yoshida, N. 2001, MNRAS, 321, 372

Jing, Y. P., Börner, G., & Suto, Y. 2002, ApJ, 564, 15

Jing, Y. P., Mo, H. J., & Boerner, G. 1998, ApJ, 494, 1

Kazantzidis, S., Mayer, L., Mastropietro, C., Diemand, J., Stadel, J., & Moore, B. 2004, ApJ, 608, 663

Klypin, A., Gottlöber, S., Kravtsov, A. V., & Khokhlov, A. M. 1999, ApJ, 516, 530

Koushiappas, S. M., Zentner, A. R., & Kravtsov, A. V. 2010, ArXiv e-prints

Kravtsov, A. V., Berlind, A. A., Wechsler, R. H., Klypin, A. A., Gottlöber, S., Allgood, B., & Primack, J. R. 2004a, ApJ, 609, 35

Kravtsov, A. V., Gnedin, O. Y., & Klypin, A. A. 2004b, ApJ, 609, 482

Kravtsov, A. V., & Klypin, A. A. 1999, ApJ, 520, 437

Lacey, C., & Cole, S. 1993, MNRAS, 262, 627

——. 1994, MNRAS, 271, 676

Lee, K., Giavalisco, M., Gnedin, O. Y., Somerville, R. S., Ferguson, H. C., Dickinson, M., & Ouchi, M. 2006, ApJ, 642, 63

Li, C., & White, S. D. M. 2009, ArXiv e-prints

Maddox, S. J., Efstathiou, G., Sutherland, W. J., & Loveday, J. 1990, MNRAS, 243, 692

Magliocchetti, M., & Porciani, C. 2003, MNRAS, 346, 186

Marzke, R. O., Geller, M. J., da Costa, L. N., & Huchra, J. P. 1995, AJ, 110, 477

Masjedi, M., et al. 2006, ApJ, 644, 54

Moore, B., Ghigna, S., Governato, F., Lake, G., Quinn, T., Stadel, J., & Tozzi, P. 1999, ApJ, 524, L19

Navarro, J. F., Frenk, C. S., & White, S. D. M. 1997, ApJ, 490, 493

Norberg, P., et al. 2002, MNRAS, 332, 827

Oguri, M., & Lee, J. 2004, MNRAS, 355, 120

Ouchi, M., et al. 2005, ApJ, 635, L117

Peñarrubia, J., & Benson, A. J. 2005, MNRAS, 364, 977

Peacock, J. A., & Smith, R. E. 2000, MNRAS, 318, 1144

Peebles, P. J. E. 1973, ApJ, 185, 413

——. 1974, A&A, 32, 197

Peebles, P. J. E., & Hauser, M. G. 1974, ApJS, 28, 19

Purcell, C. W., Bullock, J. S., & Zentner, A. R. 2007, ApJ, 666, 20

——. 2008, MNRAS, 391, 550

Ross, A. J., Percival, W. J., & Brunner, R. J. 2010, MNRAS, 407, 420

Santiago, B. X., Strauss, M. A., Lahav, O., Davis, M., Dressler, A., & Huchra, J. P. 1995, ApJ, 446, 457

Saunders, W., et al. 2000, MNRAS, 317, 55

Scoccimarro, R., Sheth, R. K., Hui, L., & Jain, B. 2001, ApJ, 546, 20

Shectman, S. A., Landy, S. D., Oemler, A., Tucker, D. L., Lin, H., Kirshner, R. P., & Schechter, P. L. 1996, ApJ, 470, 172

Smith, R. E., et al. 2003, MNRAS, 341, 1311

Somerville, R. S., & Kolatt, T. S. 1999, MNRAS, 305, 1

Stewart, K. R., Bullock, J. S., Barton, E. J., & Wechsler, R. H. 2009, ApJ, 702, 1005

Tasitsiomi, A., Kravtsov, A. V., Wechsler, R. H., & Primack, J. R. 2004, ApJ, 614, 533

Taylor, J. E., & Babul, A. 2004, MNRAS, 348, 811

——. 2005a, MNRAS, 364, 515

——. 2005b, MNRAS, 364, 535

Tinker, J. L., Weinberg, D. H., Zheng, Z., & Zehavi, I. 2005, ApJ, 631, 41

Totsuji, H., & Kihara, T. 1969, PASJ, 21, 221

Tucker, D. L., et al. 1997, MNRAS, 285, L5

van den Bosch, F. C., Tormen, G., & Giocoli, C. 2005, MNRAS, 359, 1029

Wake, D. A., et al. 2011, ApJ, 728, 46

Watson, D. F., Berlind, A. A., McBride, C. K., & Masjedi, M. 2010, ApJ, 709, 115

Wechsler, R. H., Bullock, J. S., Primack, J. R., Kravtsov, A. V., & Dekel, A. 2002, ApJ, 568, 52

White, S. D. M., & Rees, M. J. 1978, MNRAS, 183, 341

York, D. G., et al. 2000, AJ, 120, 1579

Zehavi, I., et al. 2004, ApJ, 608, 16

——. 2010, ArXiv e-prints

——. 2005, ApJ, 630, 1

——. 2002, ApJ, 571, 172

Zentner, A. R. 2007, International Journal of Modern Physics D, 16, 763

Zentner, A. R., Berlind, A. A., Bullock, J. S., Kravtsov, A. V., & Wechsler, R. H. 2005, ApJ, 624, 505

Zentner, A. R., & Bullock, J. S. 2003, ApJ, 598, 49

Zheng, Z. 2004, ApJ, 610, 61

Zheng, Z., et al. 2005, ApJ, 633, 791

Zheng, Z., Coil, A. L., & Zehavi, I. 2007, ApJ, 667, 760